14

SYNCHROTRON-BASED X-RAY AND FTIR ABSORPTION SPECTROMICROSCOPIES OF ORGANIC CONTAMINANTS IN THE ENVIRONMENT

JOHN R. LAWRENCE AND ADAM P. HITCHCOCK

14.1. INTRODUCTION

Synchrotron-based imaging and analyses represent important and increasingly accessible research tools for the analyses of complex environmental materials and their interactions with contaminants in natural systems (Bluhm et al. 2005; Dynes et al. 2006a,b; Thieme et al. 2007; Hitchcock et al. 2008b; Neu et al. 2010). Environmentally relevant processes may involve microscopically variable chemical and biological interactions that must be analysed at high spatial resolution. Synchrotrons provide many different photon energies—ranging from IR to hard X-ray—that may be applied to environmental samples. The interaction of the light with the sample may be monitored as transmission, electron, or X-ray fluorescence yield or by a wide range of elastic and inelastic scattering processes (Bertsch and Hunter 2001; Brown and Sturchio 2002). More recent studies in the soft X-ray regime have demonstrated application to environmental matrices, including isolated bacterial cells (Obst et al. 2009a,b) and biofilms (Gilbert 1999; Lawrence et al. 2003; Dynes et al. 2006a,b, 2009; Hunter et al. 2008). Application of these techniques can significantly advance our understanding of the processes controlling the chemodynamics of contaminants in the environment, including speciation, distribution, reactivity, transformations, mobility, and their potential bioavailability in the environment. This chapter introduces synchrotron-based imaging and spectroscopies and how they are used for the analyses of complex materials and their interactions with contaminants in natural systems. We will discuss X-ray absorption theory and methodology, including instrumentation, how to prepare, measure, and quantitatively analyze environmental samples, focusing on the spectroscopy, microscopy, detection and mapping of organic contaminants. The same approach will be used to cover synchrotron-based Fourier transformed infrared spectroscopy (FTIR). Examples of both techniques applied to studies of organic contaminants in the environment will be given.

Of particular interest for the environmental and biological sciences is soft X-ray scanning transmission X-ray microscopy (STXM), which was developed first by Kirz and Rarback (1985). Soft X-ray spectromicroscopy is increas-

Biophysico-Chemical Processes of Anthropogenic Organic Compounds in Environmental Systems.
Edited by Baoshan Xing, Nicola Senesi, and Pan Ming Huang.

ingly available with the rise in the number of high brightness, third-generation light sources that are equipped with STXMs, and improvements in instrumentation and data analysis (Bluhm et al. 2005; Hitchcock et al. 2008a). The STXM method uses the intrinsic properties of the sample based on the application of the near-edge X-ray absorption fine structure (NEXAFS) spectral signal (Stöhr 1992) as the analytical contrast mechanism that allows mapping of chemical species based not only on elemental composition but also on bonding structure (Ade and Urquhart 2002; Ade and Hitchcock 2008). Further, since it is a photon-in/photon-out technique, STXM may be applied to fully hydrated biological materials—soft X rays penetrate water, particularly in the critical $C1s$ spectral range (280–340 eV), where up to 3 μm of water can be tolerated. Although it has much lower spatial resolution, STXM provides significantly better analytical information than does electron energy loss spectroscopy in transmission electron microscopes (TEMs) because of its superior energy resolution, greater ability to measure thicker samples without spectral distortion, and much greater analytical signal per unit radiation damage (Rightor et al. 1997; Wang et al. 2009a,b). In the wider energy range provided by the undulator-based STXMs a core edge is available for nearly all elements. Many environmental samples, particularly in the fully hydrated state, were previously difficult or impossible to study by other means, because of inadequate spatial resolution (NMR, MRI, optical techniques), sample distortions and artifacts associated with dehydration, radiation effects (electron-beam based techniques), or a lack of suitable chemical information (scanning probe and elemental analysis techniques). In addition, STXM combines the chemical speciation sensitivity of NEXAFS spectroscopy with high spatial resolution (< 30 nm). Thieme et al. (2007, 2008) provide an overview of some potential applications of X-ray microscopy in the environmental sciences. Brown and Sturchio (2002) and Lombi and Susini (2009) provide excellent overviews of synchrotron techniques, including STXM, hard and soft X-ray NEXAFS spectroscopy, and hard X-ray EXAFS spectroscopy, as well as their applications in environmental science.

Fourier transform infrared (FTIR) absorption spectroscopy is well established; however, with synchrotron light as the source, versus conventional light sources, both the detection limit and spatial resolution have been substantially improved, resulting in the development of improved spatially resolved FTIR spectromicroscopy. Although FTIR spectromicroscopy is well suited to research on environmental topics, given its excellent capacity to detect organic molecules, its spatial resolution is only in the micrometer range. Excellent overviews of the essentials of IR and IR microspectroscopy have been prepared by a number of authors covering biomedical application (Miller et al. 2003; Dumas and Miller 2003), bacterial cells, (Naumann et al. 1996), applications of geochemistry and environment sciences (Hirschmugl 2002a,b; Rash and Vogel 2004; Holman and Martin 2006; Lombi and Susini 2009). In addition, an article in Research: Science and Education by M. Stern (Stern 2008) in combination with material by Miller (2010) provides an excellent entry point to synchrotron FTIR spectromicroscopy.

In the following review the reader will be provided with information regarding the beamlines available world wide for carrying out these techniques. We will explain how these techniques are rapidly developing as powerful analytical tools for studies in the biological and environmental sciences because they offer chemically sensitive imaging with which to interrogate samples and, in the case of STXM, high spatial resolution. Infrared microscopy can directly map organics in a sample but is much more limited by spatial resolution. Discussion of applications to the detection and mapping of the major biomolecules (protein, lipids, polysaccharides, carbonate, and nucleic acids) and their characteristic spectra will be provided. Software available for the handling and processing of data collected will be described. We will present a critical review of the literature, providing examples of the successful application of these techniques to visualization and mapping of organic contaminants in environmental matrices. The chapter will also highlight future research needs and directions.

14.2. SCANNING TRANSMISSION X-RAY MICROSCOPY (STXM)

In STXM, images are obtained in a pixel-by-pixel fashion by mechanically raster-scanning the sample through the focal point of a zone plate X-ray lens (or in some instruments, scanning the zone plate with the sample stationary) while detecting the intensity of the X rays transmitted through the sample (see Fig. 14.1). The quality of the zone plate is critical since the spatial resolution (Rayleigh criterion) of a perfect amplitude contrast Fresnel zone plate is 1.22 times the outermost zone width (Howells et al. 2007). The best zone plates in present-day soft X-ray STXMs have an outermost zone width of 15 nm, which provides a demonstrated spatial resolution of 18 nm (Vila-Comamala et al. 2009). Zone plates with 25 nm outer zone widths have been used in third order, achieving better than 15 nm spatial resolution (Tyliszczak 2010, private communication). There have been great improvements in zone plate fabrication methods and thus quality over the past few years, giving rise to expectations of ultimately achieving a spatial resolution in first order of > 10 nm.

14.2.1. Instrumentation and Access to STXM

Soft X-ray imaging and spectromicroscopy with STXM has been carried out at a number of facilities, including two-microscopes at the National Synchrotron Light Source

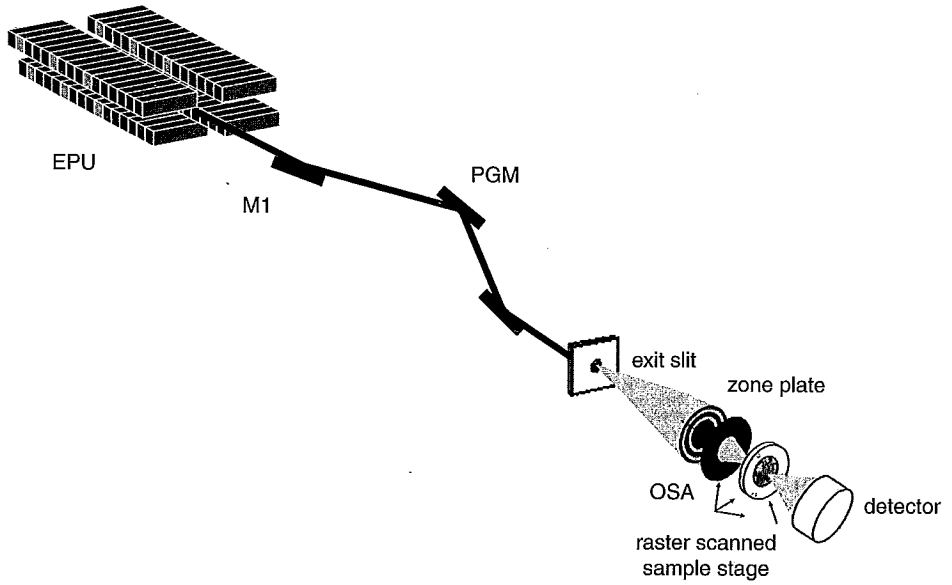

Figure 14.1. Schematic (not to scale) of 10ID1 beamline and STXM at the Canadian Light Source (CLS) (EPU—elliptically polarizing undulator; M1,M3—mirrors; PGM—plane-grating monochromator; OSA = order-sorting aperture; exit slit also acts as a spatial coherence filter.

(NSLS), two (soon to be three) at the Advanced Light Source (ALS) (Kilcoyne et al. 2003), the Canadian Light Source (CLS), Elettra (Italy), and the Swiss Light Source (SLS). In addition, beamlines are under construction at the Stanford Synchrotron Light Source (SSRL, United States), Bessy (Berlin, Germany), SSRF (Shanghai, China), Soleil (Paris, France), Alba (Barcelona, Spain), and Diamond (Oxford, UK). In addition, STXMs covering the tender X-ray regime (2–8 keV) are available at each of the three third-generation high-energy rings: European Synchrotron Facility (ESRF), Argonne (APS), and Spring8. Some of these STXM installations have been the subject of detailed presentations with examples of their applications. For example, the STXM on the molecular environmental science beamline 11.02 at ALS has been reviewed by Bluhm et al. (2005), while Hitchcock et al. (2008a) provided an overview of the spectromicroscopy facility at the Canadian Light Source (CLS) in Saskatoon, Canada. The source point may be a bending magnet, linear undulator, or an elliptically polarized undulator (EPU) such as at the CLS. In the case of the CLS (Fig. 14.1), the X-rays are directed by a sagittal cylindrical mirror to a plane grating monochromator that allows performance over an energy range from 150 to 2500 eV (Hitchcock et al. 2008a); this instrument currently has the broadest energy range available for soft X-ray STXM applications. Most STXM analyses use the information provided by the NEXAFS of elements with absorption edges in the soft X-ray energy range, in particular the carbon, nitrogen, and oxygen K edges. The K-shell absorption edges of Na, Mg, Al, and Si and the L edges of important transition metals including Ti, V, Cr, Mn, Fe, Co, Ni, Cu, and Zn, as well as the L edges of P, S, Cl, K, and Ca, are all available. For heavier elements there are other absorption edges, which can be accessed at STXM beamlines.

The ability to clearly resolve hydrated samples at high magnification, with a resolution of 30 nm and with minimal sample preparation, are powerful features of STXM. Limitations to STXM include radiation damage, a requirement for very thin samples (<200 nm equivalent thickness of dry organic components), the presence of less <5 μm of water when wet, use of fragile silicon nitride windows (other options, such as formvar or polyimide, are available as described below), challenging sample preparation (i.e., encapsulation in a wet cell and absorption saturation distortion of analysis in thick regions of a specimen) and suitability of model compounds used to create reference spectra for quantitative mapping. Despite these limitations, STXM has been used for a wide variety of sample matrices, including those that are polymeric, geochemical, magnetic, extraterrestrial, biological, and environmental.

14.2.2. Sample Preparation

All STXM samples must be prepared either freestanding (typically draped across a 3-mm Cu grid as used in electron microscopy), or on an X-ray transparent holder; STXM measurements can be performed on a wet cell constructed by sandwiching the sample between two thin (50–100-nm) silicon nitride windows (Norcada Inc, Edmonton AB, Canada; Silson Inc, Northampton, UK). In the case of biological materials, samples may be grown directly on the window (Lawrence et al. 2003; Dynes et al. 2009).

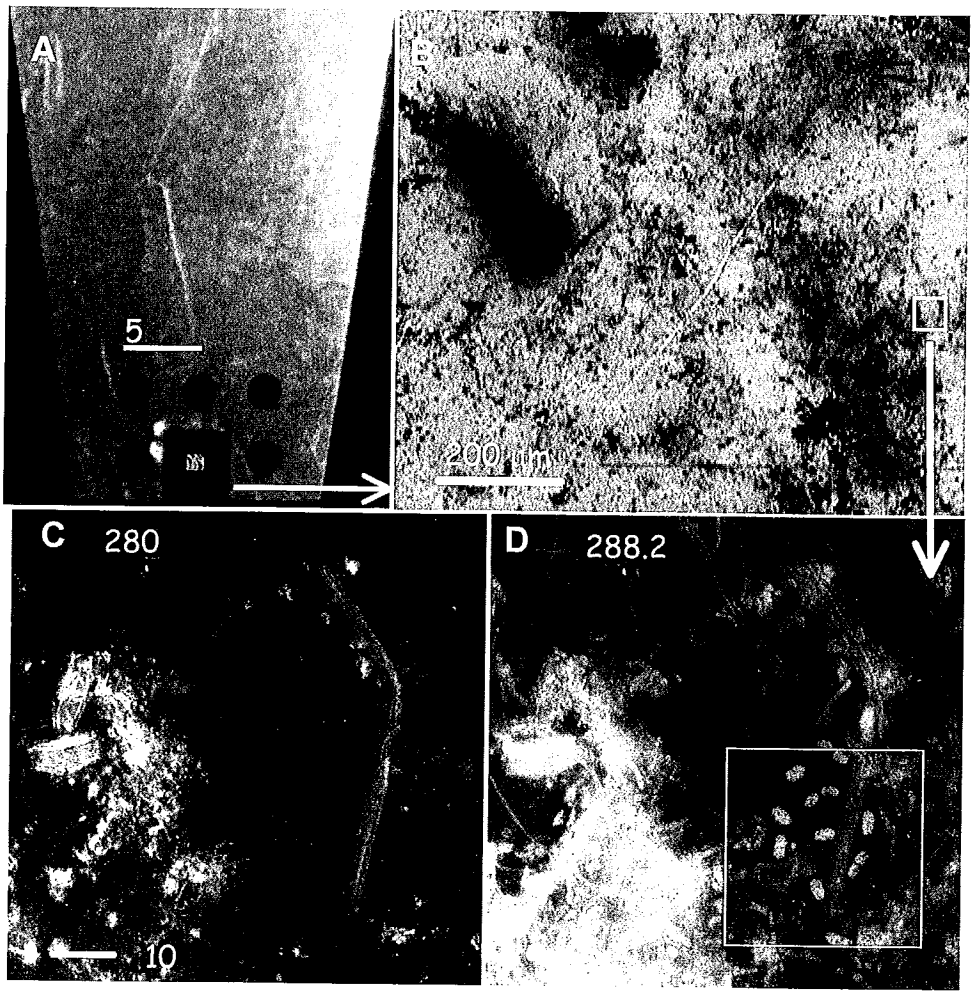

Figure 14.2. (a) Photograph of a wet cell mounted on a STXM sample plate of the type used at the ALS, CLS, and SLS. Up to six samples can be mounted on a single STXM plate. (b) STXM image (transmission) at 288 eV of the whole 1-mm silicon nitride pane (2 × 75 nm) and the enclosed natural river biofilm sample. (c) STXM image (optical density, OD) of an 80 × 80 μm area of the biofilm at 280 eV, below the *C*1*s* absorption onset, where inorganic species (silica, calcium, etc.) are highlighted. (d) STXM image (OD) of the same 80 × 80 μm area as in (c) at 288.2 eV, the peak of the $C1s \rightarrow \pi^*_{amide}$ transition of proteins that highlights biological species. The white box indicates the region subjected to detailed *C*1*s* image sequence, with analysis results presented in Figure 14.4.

Figure 14.2 shows a typical completed silicon nitride window wet cell with enclosed sample mounted on an aluminum holder placed in the microscope. It is also possible to construct wet cells using polyimide windows (Luxel Corporation, Friday Harbor, WA, http://www.luxel.com/). Relative to silicon nitride, polyimde is less brittle, making it an easier-to-handle window system that may be more amenable to environmental samples (Hitchcock et al. 2008a). Although polyimide windows have *C*1*s* signals, it is characteristically and radiation-stable. Also, for the 30-nm polyimide used, the absorbance in the *C*1*s* region (280–300 eV) is much lower that that of Si_3N_4 windows. This allows analysis of thicker samples before absorption saturation becomes a limiting factor. This is of particular advantage for use with biological and environmental samples such as microbial biofilms. Although a wet cell may be preferred for many applications, the samples may also be mounted on a suitable substrate (window or coated grid) and air-dried prior to being examined dry. In many cases this is a straightforward process and allows imaging and data collection without the complications of maintaining a wet cell, although there can be concerns about modification of the sample on dehydration. For example, Obst et al. (2009a) simply deposited 1–2 μL of a cyanobacterial cell suspension onto a Si_3N_4 window (1 ×

1 mm, thickness 100 nm on a 200-μm-thick Si chip, 5 × 5 mm, Norcada Inc., Edmonton, Canada) and then used a filter paper to withdraw free water leaving the cells on the window surface. Use of bibulous papers (available from a number of suppliers, e.g., Fisher Scientific, Wards Natural Science) may also be considered as they provide greater control over the rate of water removal.

Although observation of unaltered, fully hydrated materials is highly desirable, the necessity for special handling and preparation may also prevent it. In many cases the sample may be too thick for STXM, thus requiring embedding in epoxy (Spurr's resin), or nanoplast (Lawrence et al. 2003). However, fixation, alcohol dehydration and embedding in epoxy resins removes most of the organic biological compound, and the spectrum of the embedding material masks the *C1s* spectral information of the sample as shown by Lawrence et al. (2003). Therefore approaches such as cryosectioning, in which the sample is frozen and sectioned, may be preferable to conventional electron microscopy sample preparation for environmental applications (Lawrence et al. 2003). Thin sections or ultrathin sections may be placed on a silicon nitride or polyimide window or on electron microscope grids for mounting and observation in STXM. Figure 14.2b illustrates a typical arrangement of samples on windows attached to an aluminum sample plate or holder. In another useful approach for specific sample types, Loo et al. (2001) describe the use of glycolmethacrylate-embedded and sectioned materials for STXM analyses.

Sulfur embedding has been highly successful for embedding interplanetary dust samples (Bradley et al. 1993); it has also been used in conjunction with soil aggregates (Lehmann et al. 2005). Essentially, particles are embedded in preheated (220°C) elemental sulfur and supercooled (in liquid N_2) before sectioning, imaging, and spectroscopic analysis. Lehmann et al. (2005) and Kinyangi et al. (2006) provide a detailed description of the technique. This approach has the advantage of being carbon-free; however, sublimation at room temperature limits longer-term storage or examination under vacuum.

Another option for environmental samples used to observe mineral interfaces is that of focused ion beam (FIB) milling, which allows for careful selection of the slice plane. Obst et al. (2005, 2009a) illustrates the preparation of ultrathin sections of $CaCO_3$ crystals attached to cyanobacteria by FIB milling using the liftout approach. Essentially, the material is air-dried, coated with platinum to protect the organic material, and then sectioned using an optimized approach to minimize damage to the specimen (Obst et al. 2005). The prepared ultra thin sections may then be transferred to carbon-coated 200-mesh copper TEM grids using a micromanipulator.

In addition to conventional 2D imaging of samples, it is possible to perform 3D imaging using STXM, employing either serial section (Hitchcock et al. 2003) or angle scan techniques. Johansson et al. (2007) described an apparatus that enables rotation of samples at the focus of the X-ray beam in a STXM, allowing measurement of 3D chemical distributions with ~50 nm spatial resolution in three dimensions. Samples can be placed in thin-walled glass capillaries similar to those typically used as micropipettes in intra- and extracellular physiology, or on strips of conventional copper grids. Prior to loading of a sample, the capillaries must be treated by heating and pulling using a micropipette puller to reduce the initial diameter of 1 mm to ~2–3 μm with a uniform wall thickness in the range of a few hundred nanometers over the length to be scanned by STXM of approximately 10–20 μm. These capillaries may then be filled with the sample, either from the top, or from the end of the thin section, using capillarity. The method has been used to study yeast cells, bacterial cells, biofilm communities, and synthetic polymer samples (Johansson et al. 2007). After filling with the wet sample, the capillaries are centrifuged for 5–10 min at 6000*g* to ensure that the water and the sample move into the fine tip. The capillary is then sealed with silicone (RTV silicone, WPI, Sarasota, FL). However, imaging may be best done using *O1s* edge rather than *C1s*. In another option, Hitchcock et al. (2008b) described the use of a carbon tube with 45-nm walls and an internal diameter of <1 μm in the region of the sample. Use of these sample containers allowed imaging at the *C1s*. In this case, rather than centrifuging the samples, they were able to add the sample via capillarity. The capillary end was sealed with silicon grease prior to imaging in the STXM.

Cell biologists have demonstrated that 3D reconstructions of data measured using the closely related full-field transmission X-ray microscopy (TXM) from individual cells have excellent natural contrast, eliminate the need for staining, and reveal additional details of intact cells in a near native state (Gu et al. 2007; Larabell and Le Gros 2004; Parkinson et al. 2008). Some of the best examples of this application are the imaging and reconstruction of whole, fully hydrated yeast cells *Schizosaccharomyces pombe* (Parkinson et al. 2008) and the 3D imaging and mapping of 1-μm acrylate-filled spheres (Johansson et al. 2007; Hitchcock et al. 2008b). Figure 14.3 illustrates five of a series of STXM projection images of a biofilm sample at different angles. A set of 26 such images was used to create a 3D reconstruction of a river biofilm community containing a diatom mounted in a capillary (Johansson et al. 2006). Thieme et al. (2003) present tomographic reconstructions of bacteria and colloids revealing detailed information on spatial arrangements. This approach holds considerable promise for 3D chemical mapping of biological and environmental samples.

14.2.3. Imaging and Data Collection

After preparation, the wet cell, grid, or window is mounted on a aluminum holder plate, allowing it to be placed directly in

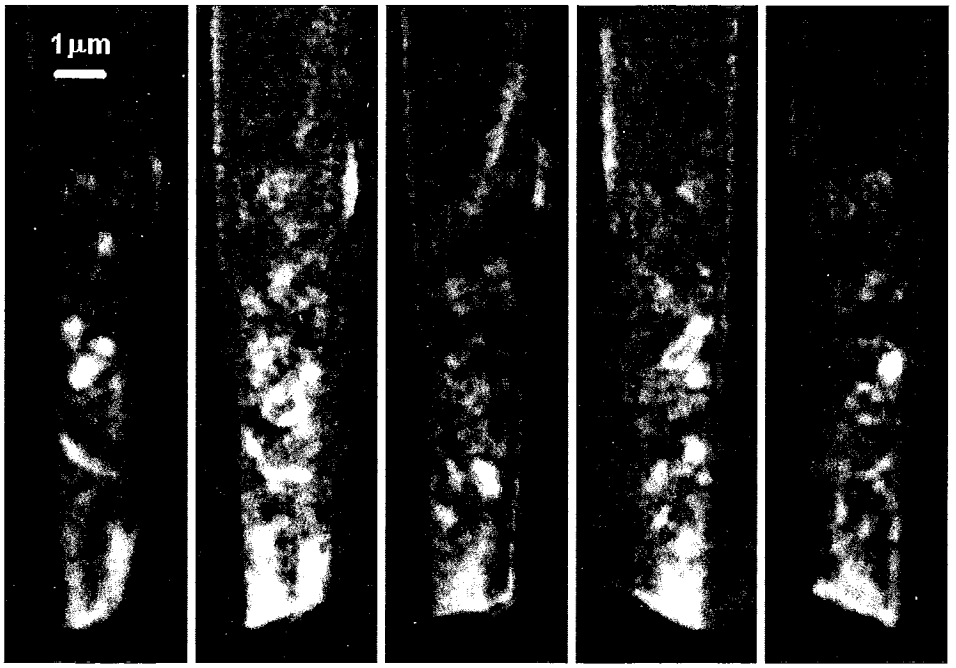

Figure 14.3. Chemical maps of "protein" in a 3D volume—selected slices from a 3D reconstruction of the protein component of a wet river biofilm, derived from the difference of 2D projection images recorded at 532.2 and 530.0 eV.

the beamline for imaging (Lawrence et al. 2003; Hitchcock et al. 2002) (see Fig. 14.2). The sample is placed in the STXM chamber connected to the beamline, and moved to the focus of the zone plate. The sample chamber is then evacuated (if the sample is dry) or purged with dry helium (for sealed wet cells) prior to making measurements. Modern STXMs (Feser et al. 2000; Kilcoyne et al. 2003) have high-precision mechanical and piezoelectric scanning systems with interferometry-based control, allowing ranges of sample positioning and scanning from < 1 m to several centimeters, with nanometer precision. For scans made with the fine piezo stage, dwell times can be as fast as 100 μs/pixel, although 1 ms/pixel is more typical for analytical results. Data acquisition of images larger than the range of the fast piezo stage use stepping motor-driven stages, which are much slower than the piezo stages. Use of an indexed optical microscope can help to rapidly identify areas of interest and thus use beam time most efficiently. Between the zone plate and the sample there is the order selection aperture (OSA), a 30–100-μm-diameter aperture placed so as to block zeroth-order light (in conjunction with the central stop of the zone plate) but not to clip the focused first-order diffracted light. Proper alignment of the OSA and central stop is required to achieve high-spatial-resolution images and valid spectroscopy at the ultimate spatial resolution.

Depending on the instrument, the transmitted X rays are detected by a proportional counter (NSLS), a Si photodiode (CLS), a segmented photodiode [NSLS (Feser et al. 2000)], an avalanche photodiode (ALS), or a phosphor scintillator, and a photomultiplier tube [ALS, CLS (Kilcoyne et al. 2003)]. It is necessary to check the energy scale daily, particularly at the undulator beamlines at ALS and CLS, which do not have entrance slits and thus rely on reproducibility of the storage ring beam position. The energy scale can be established to a precision of ±0.05 eV using sharp gas-phase signals, typically the Rydberg peaks of gases such as N_2, CO_2, O_2, and Ne. Calibration may also be carried out using other standard samples, including various solids such as Si, SiO_2, and Al_2O_3.

Additional details and explanations of beamline design, construction, and operation are provided in Kilcoyne et al. (2003), and Bluhm et al. (2005), while soft X-ray optics are dealt with by Jacobsen et al. (1991, 1992). A number of excellent reviews (Ade 1998; Ade and Urquhart 2002; Kirz et al. 1995, Howells et al. 2007; Ade and Hitchcock 2008) can be consulted for more technical details on the optics and mechanics of transmission X-ray microscopes, as well as comparisons of STXM to the three other common soft X-ray synchrotron spectromicroscopies—full-field transmission X-ray microscopy (TXM), scanning photoelectron microscope, and photoemission electron microscopy.

The STXM technique can be used analytically by acquiring NEXAFS spectra at a single point, using a spectral line scan, or through collection of a sequence of images at different energies, often referred to as a "stack" (Jacobsen et al. 2000). The range and point spacing of the energy scale

are selected in order to differentiate the chemical components of interest in the sample. Monochromatic soft X rays are absorbed by the sample at specific energies at which core electrons are excited to unoccupied states, with intensities and linear dichroic properties characteristic of the chemical species being excited (Stöhr 1992).

The acquisition of a full STXM dataset consisting of an image sequence of $\sim 4 \times 4\,\mu m^2$ area, sampled at 40 nm (100×100 pixels) with 1 ms/pixel dwell and 120 energy steps, takes 30 min, with perhaps another 30 min spent in initial focusing, navigating to a suitable area, and making higher-quality single energy images. If one wants very good statistics, higher spatial sampling (for some projects, pixels as small as 5 nm are used to oversample particular areas) or if multiple core levels are studied, a single sample can take 4 h or more to measure. Prescreening conventional light or laser light microscopy, or even transmission electron microscopy under low-dose conditions (for dry samples) is very useful for make a strategic selection of areas for STXM analysis. With this prescreening, the user will collect single-energy images at selected energies for navigation within the sample and ultimate selection of the sites of interest for detailed STXM imaging.

In some cases it is useful to employ a full-spectrum sampling strategy, particularly with samples that are poorly characterized and may contain unknowns. Figure 14.4 shows a selection of images from a 52-image sequence of a wet river biofilm, recorded using 233×233 pixels and 1 ms/pixel dwell. In order to improve statistics, images in regions with similar spectral characteristics are summed, and some differences are taken to emphasize the chemical contrast. A more complete, quantitative analysis of this image sequence using spectral fitting techniques has been presented elsewhere (Hitchcock et al. 2005). These types of STXM image sequences contain much analytical information, but they must be processed correctly to extract valid results. The measured transmitted signals (I) are first converted to optical densities [absorbance, OD = -ln(I I0-1)] using incident flux (I0) measured through regions of the wet cell devoid of biofilm/sample, to correct for the absorbance by the silicon nitride membranes and the water in the wet cell. Following this conversion, a number of strategies may be used to extract quantitative chemical maps and to interrogate the reliability of the results. Some of these are discussed below.

Although STXM provides much more information per unit damage as compared to TEM-EELS (Rightor et al. 1997; Wang et al. 2009a), it uses ionizing radiation, which does result in radiation damage to samples, particularly if long dwell times or many energies are used, or if a number of core edges are measured at the same location. Various organic compounds may be modified by ionization and dissociation of bonds (Cody et al. 2009; Wang et al. 2009b). A useful strategy to monitor the level of damage in any given measurement is to collect a postsequence image over a region centered on, but a few micrometers larger than the main stack area. Since the raster scan starts at zero velocity, an additional dose is given to a $\sim$1-μm section just to the left of the area where the stack is measured, which forms a clear vertical stripe, if the damage is extensive (see Fig. 14.5, which shows damage visualization in a radiation-sensitive PMMA sample). In examining larger scale images it is possible to focus on two regions where damage is most likely to have occurred, the STXM operates in a line-at-a-time mode; therefore, the beam sits $\sim$1 μm to the left of the start position of each horizontal scan line for about 10 times longer than in any pixel in the stack; similarly, there is a deceleration region at the right side of the stack. Damage will be clearly visible within a vertical zone outside the area in which the stack was collected.

Typically for each system there is one component more damage sensitive than others. Post image sequence imaging at the energy where the damage to that component is most visible is a good way to check whether any given measurement was made within acceptable limits of sample damage. For example, in microbial biofilm systems a damage check scan is typically measured at 289 eV to detect changes to polysaccharides, the most easily damaged chemical component. We are willing to accept data for further workup if the extracellular matrix polysaccharide signal is reduced by less than 20% (Dynes et al. 2006b). Toner et al. (2005) demonstrated that radiation damage in STXM can modify oxidation-state speciation (e.g., Fe 2*p* and Mn 2*p*). In addition to monitoring for damage, it is useful to establish the potential for damage in the STXM beamline by assessing the stability of the material under examination. Wang et al. (2009b), Cody et al. (2009), and others have discussed in detail radiation damage mechanisms in polymer and biological samples in a special issue of *Journal of Electron Spectroscopy and Related Phenomena* (February 2009). There are also strategies to minimize radiation damage, including defocusing the X-ray beam (with appropriately matched pixel spacing) or short dwell times and very restricted energies (which works well once a good understanding of the spectral–speciation relationship for a class of samples has been achieved). In addition, a strategy of extrapolating back to the unaltered spectrum at zero time may also be possible. However, one must note that, even if there is not evidence of damage at a particular energy due to destruction or formation of a bond absorbing at the energy or from mass loss (ablation), this does not mean that damage has not occurred.

14.2.4. Quantification

After collection of the image sequences, additional processing is required before quantitative analyses can proceed. This includes alignment of images (if needed), conversion to

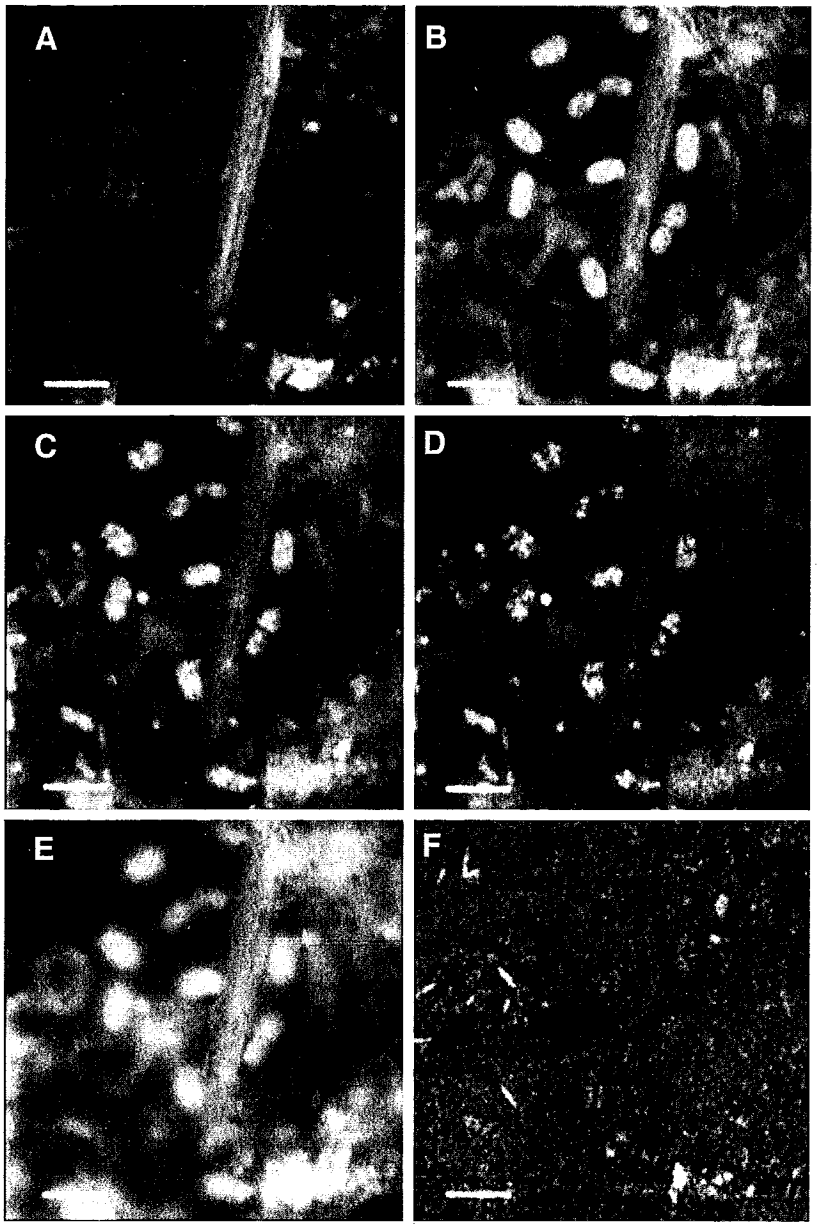

Figure 14.4. STXM images of a wet river biofilm: (a) sum of 12 images (282.0–286.0 eV)—inorganic species including SiO_2 of a diatom frustule and $CaCO_3$; (b) sum of two images (287.5–288.3 eV)—protein amide π^*; (c) sum of three images (288.53–288.9 eV)—lipids and protein; (d) image (c) minus 0.5* image (b)—lipids; (e) sum of 10 images (290.0–294.0 eV)—carbohydrates, lipids, and proteins; (f) sum of six images (296.5–301.0 eV) minus image (e)—potassium. Scale bar is 5 μm. Further results on this sample were presented in Hitchcock et al. (2005).

optical density, and removal of any single images where the spectral content statistically deviates from the local trend (glitches). The images can be aligned using 2D Fourier autocorrelation techniques or by manual alignment procedures. There should be minimal drift from image to image. To check alignment, images may be summed to assess whether objects shift or change size within the stack. The processed image sequence data can then be converted to component maps (distributions of distinct chemical species, e.g., proteins, polysaccharides, nucleic acids, organic or metallic components) by spectral fitting using linear regression procedures. Each of the spectro-microscopic datasets consists of many thousands of NEXAFS spectra (one per pixel of the analyzed area). These spectra represent the sum of the spectral contributions of all the individual chemical species that are present at this spot of the sample (i.e.,

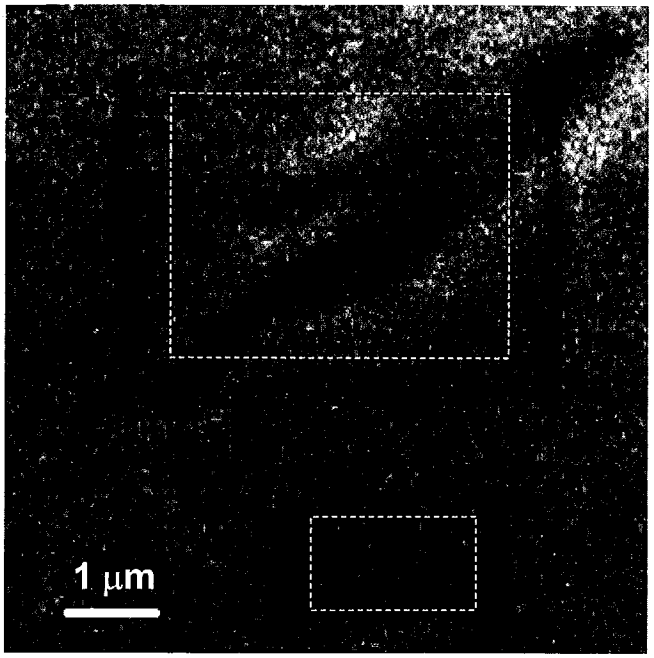

Figure 14.5. Postanalysis imaging of a polymethylmethacrylate (PMMA) thin film over an area larger than the scan used (white dashed lines) reveals vertical lines to left and sometimes to right of the imaged area, which are due to the greater exposure in the region of each line used for accelerating and decelerating the sample during each line scan.

typically 10^4–10^5 spectra). These datasets are best analyzed using efficient, matrix-based least-squares techniques such as singular value decomposition (Koprinarov et al. 2001, 2002) or by multivariate statistical methods such as principle components and cluster analysis (Jacobsen et al. 2003; Lerotic et al. 2005, 2004; Mitrea et al. 2008). A graphical user interface implementing many different data analysis protocols and with ability to read in most spectromicroscopy data formats is freely available (Hitchcock 2009).

In a relatively typical case involving the application of singular value decomposition (SVD) an image sequence was recorded, which consisted of 160 images between 280 and 320 eV, each of dimension 300 × 125 pixels, collected with a dwell time of 1 ms/pixel (total acquisition time, including "dead" time to return the piezo scanner to the star to the next line was 2.5 h) (Dynes et al. 2006a). Quantitative maps of chlorhexidine, protein, lipid, polysaccharide, silica (SiO_2), CO_3^{2-}, and K^+ were then derived from this image sequences by using SVD (Dynes et al. 2006a; Pecher et al. 2003: Koprinarov et al. 2002; Jacobsen et al. 2000) to fit the spectrum at each pixel to a linear combination of reference spectra of the components suspected to be present. The reference spectra used in this case are displayed in Figure 14.6 (Dynes et al. 2006a). Quantitative reference spectra were determined using human serum albumin (protein), 1,2-dipalmitoyl-*sn*-glycero-3-phosphocholine (lipid), xanthan gum (polysaccharide), and K^+ (K_2CO_3 with the signal of $CaCO_3$ subtracted to remove the *C*1*s* spectrum of the carbonate anion) (Dynes et al. 2006a,b). Other reference spectra may be found in the literature. As described by Dynes et al. (2006a,b), the reference spectra recorded from pure materials, are placed on absolute linear absorbance scales by matching them to the predicted response for the compound according to its elemental composition and density, using tabulated continuum absorption coefficients (Henke et al. 1993). Each component selected for analysis requires specific data treatment. In the case of potassium K^+ it was necessary to subtract the appropriately weighted spectrum of KCO_3, from that of K_2CO_3, allowing independent derivation of a reference spectrum for pure K^+. Silica (SiO_2) presents a spectrum that is a slowly varying and featureless signal in the *C*1*s* region as taken from tabulated elemental absorption coefficients (Henke et al. 1993) and the composition and density of SiO_2. The frustules in this diatom sample were nearly pure ($\sim$ 97%) hydrated silica (SiO_2) (Noll et al. 2002) and were the dominant nonorganic component of this sample type. Therefore the component maps derived from fitting the silica component represented the spatial distribution of SiO_2. Then Ca^{2+} was mapped from the difference in optical density (OD) images at 352.6 eV (Ca $2p_{1/2} \rightarrow$ Ca $3d$ resonance) and at 350.3 eV (in the dip between the $2p_{3/2}$ and $2p_{1/2}$ resonances). The OD scale was rendered quantitative by scaling by $0.10(2)\,nm^{-1}$, the difference in the linear absorbance of nm of $CaCO_3$ at these two photon energies. The image and spectral processing may be carried out using a number of software packages, with two of them, aXis2000 (Hitchcock 2009) and the suite of IDL programs provided by Chris Jacobsen (Jacobsen 2009), written explicitly to analyze soft X-ray spectromicroscopy datasets. For most confidence in the analysis result, it is prudent to explore the reliability of any given component mapping using several approaches. The first check is a residual image, which is the difference between fit and data at each pixel, averaged over the image sequence energy range. Typically a good fit has a low magnitude and absence of structure in the residual image. A second check is to examine the fit of the spectrum of "hot spots" identified by applying a threshold masking technique to each component map, extracting the spectrum from these selected component-rich pixels, then examining the quality of the spectral fit using the same reference spectra used to generate the components. A third check is to use principal component analysis (PCA) to assesses the number of chemical components that are reasonably identifiable from a given image sequence, based solely on the variance and the statistical precision of the data.

In some instances, although rarely in environmental samples, all chemical species are known and therefore may be detected and quantified in the dataset. However, this

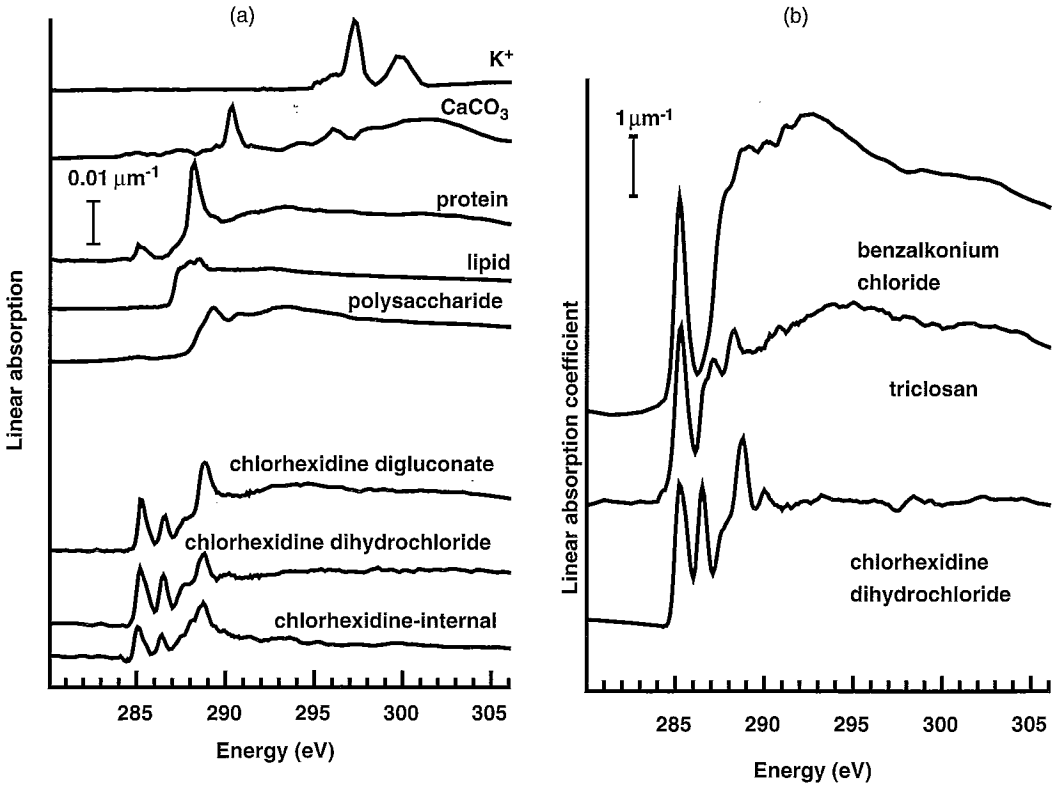

Figure 14.6. (a) *C1s* reference spectra used for analysis of chlorhexidine in an environmental river biofilm sample from [Dynes et al. (2006a) reproduced with permission]; (b) comparison of *C1s* spectra of three common antimicrobial compounds.

approach is seldom possible. Lerotic et al. (2004, 2005) have developed multivariate statistical analysis (MSA) procedures to analyze spectromicroscopy data. The image sequence was first subjected to PCA in order to orthogonalize and noise-filter the data. They then applied cluster analysis to classify the principal components to obtain rotated principal components that should correspond to the spectra of the dominant chemical components in the region studied. The cluster analysis classifies pixels according to their spectral similarity. The classification can be improved by the applying of an angle distance measure rather than the Euclidian distance measure first used (Lerotic et al. 2005). These derived spectra are then used in a target analysis (similar to SVD) to obtain thickness maps of the components. Essentially, this approach allows the user to extract representative, cluster-averaged spectra and then perform a spectral–spatial decomposition using those internally generated reference spectra. While this method is very attractive in that it is "unsupervised" (i.e., it makes no assumptions about the chemistry or spectroscopy of the sample) it has its own limitations; (1) the cluster analysis is not unique, but depends on various parameters in the implementation; and (2) whenever two chemical components have very similar spatial distributions, the cluster procedure cannot differentiate them. In such cases, if one chemical species is known to be present in the sample, its introduction at the target analysis set can frequently improve the final result.

A simple application of PCA is to determine how many components may be meaningfully extracted from any given dataset. Dynes et al. (2006a) used this approach to find that up to eight components could be meaningfully extracted from the stack for which the analysis results are displayed in Figure 14.6. Meaningful spectral fits were achieved with six (protein, polysaccharide, lipid, chlorhexidine, SiO_2, and $CaCO_3$), seven (same as for six, plus K^+), and for eight components (same as for seven, plus water) for each image sequence. Dynes et al. (2006a) also examined the application of several alternate model compound spectra for detection and mapping of the protein, polysaccharide, lipid, and chlorhexidine components in the stacks. Figure 14.7 illustrates the results of successful fitting of the reference spectra plotted in Figure 14.6 to the image stack of the diatom and bacterial colony. It shows the maps of protein, lipid, chlorhexidine, polysaccharide, CO_3^{2-}, K^+, silica and Ca^{2+} as derived by SVD. Figure 14.8 presents several false-color composites that show the distributions of the chlorhexidine in relation to other components such as lipid and polysaccharides. Similarly, Obst et al. (2009a) analyzed *C-1s* image sequences measured from samples of *Synecococcus leopoliensis* by using SVD to fit reference spectra for

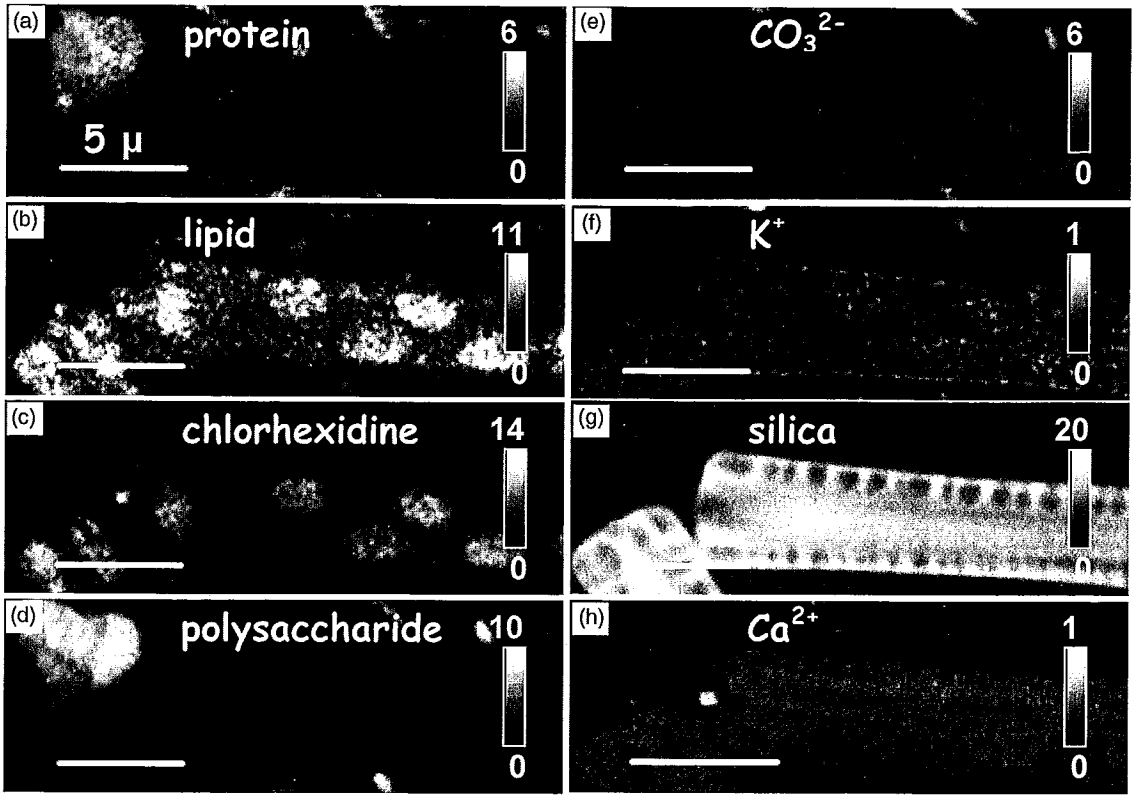

Figure 14.7. Quantitative component maps for protein, polysaccharide, lipid, chlorhexidine, K^+, SiO_2, and $CaCO_3$, plus Ca^{2+} (from the Ca 2p edge) for a river biofilm in the region of a pennate diatom cyanobacterium. [From Dynes et al. (2006a), reproduced with permission.] The gray scale gives thickness in nanometers.

protein, polysaccharides, lipids, carbonate, and the spectrum of H_2O, which has no spectral features at the *C*1*s* edge. This type of multistep evaluation supports the conclusion that the final result reported is relatively independent of the analysis used.

There remains the question of reproducibility and sensitivity in measurements of this type. Typically the spatial distributions derived in SVD analyses are surprisingly insensitive to small changes in the data range used or the reference spectra chosen (as long as they have the characteristic peaks at the correct energies). Although the precision of any single image is typically only ~2–5%, the point-to-point precision of the derived component maps is much better, due effectively to integration of the signal contributions from many images over the whole spectral range measured. However, the magnitudes of the thickness scales are considerably more variable (for weaker components, fluctuating by factors of 2). An evaluation of the variability (systematic error as opposed to random error) with different choices of reference spectra (all plausible) would assign approximately 20% uncertainty for the majority of components (maximum contributions >50 nm), and up to 50% uncertainty in the scales for the minority components (maximum contributions <50 nm). The major contribution to this uncertainly stems from systematic errors in knowing the reference spectra appropriate for a specific sample.

Another major concern with any analytical approach is its sensitivity. In general, STXM can provide quantitative maps of chemical species at environmentally relevant total concentrations (i.e., mg/kg or lower), as long as the minority components are spatially localized. (Rightor et al. 2002; Hitchcock et al. 2002; Lawrence et al. 2003). When examining biological samples, it is relatively straightforward to discriminate the major biomacromolecules, including protein, lipid, and polysaccharides. Discriminating within these categories has proved more complex. Obst et al. (2009a) noted that the chemical sensitivity of *C*1*s* spectromicroscopy did not allow detection of any major differences between the spectra obtained from EPS of cells cultured under varying nutrient conditions. In contrast, Stewart-Ornstein et al. (2006) found that it was possible to discriminate an antimicrobial peptide in a protein (albumin) background using STXM. This was based on the distinctive nature of the NEXAFS spectra of proteins that are richer in cysteine or methionine relative to other proteins. Differentiation of

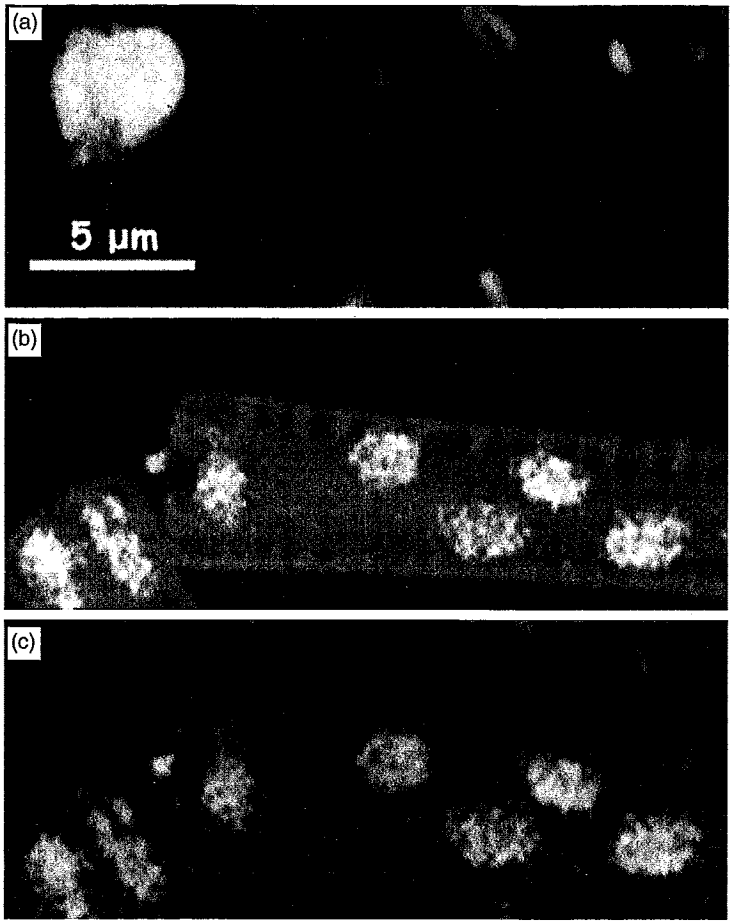

Figure 14.8. Color-coded composite maps (in each case with rescaling within each color) assembled from the component maps presented in Figure 14.7. [From Dynes et al. (2006a), reproduced with permission.] (*See insert for color representation of this figure.*)

specific peptides from a protein background has been used in studies of competitive absorption to candidate biomaterials (Leung et al. 2008).

Dynes et al. (2009) estimated the detection limit for measuring chlorhexidine by STXM by adding the spectra of chlorhexidine and the major biomacromolecules over a range of compositions and evaluating the detection limit by factoring in the visibility of the characteristic sharp features at 285.1 eV ($C1s \rightarrow \pi^*_{\text{ring}}$) and 286.4 eV ($C1s \rightarrow \pi^*_{\text{C=N}}$) transitions in the phenyl and imide groups of chlorhexidine against the background spectrum of the other species. Chlorhexidine was detected at 10 nm in the context of 50 nm of protein or 100 nm of lipid, and at a level of 20 nm against a background spectrum of 50 nm protein plus 100 nm of lipid. In this case the absolute sensitivity was impressive; corresponding to $\sim 10^{-17}$ mol, assuming that the density of pure CHX was 1.2 g/cm^3. Thus, provided accurate reference spectra are available, there is exceptional potential for the detection of organic contaminants in a relatively complex matrix using STXM.

14.2.5. Correlative Microscopy

The use of STXM in conjunction with other spectromicroscopic imaging approaches, and with light and electron microscopies, is also possible. Lawrence et al. (2003) demonstrated the application of confocal laser scanning microscopy, TEM, and STXM to the same biological samples. Dynes et al. (2006a) demonstrated the combination of CLSM and STXM to map biomacromolecules and an organic contaminant in river biofilms. The development of beamlines with "universal" mounting systems and cross-referenced sample locations for ease of navigation to regions of interest also supports the notion of the application of correlative and multimicroscopies to all types of samples, including those of environmental origin. These combinations will allow extraction of the maximum in information from an environmental sample. Schafer et al. (2007) provides a useful example of the correlative application of three different methods, TEM, STXM, and μ-FTIR microscopy, to characterize and map colloidal and particulate organic matter obtained from a lake

and two rivers. They identified the sources of colloidal material in the receiving lake environment and examined aspects of their stability, interactions, and fate. Some examples of those results are presented below.

14.2.6. Examples of STXM Applied to Organic Environmental Contaminants

Although the full potential for applications of STXM in the environmental sciences is only now emerging, there are already good examples across a range of relevant disciplines, including geochemistry, hydrology, microbiology, and atmospheric and soil sciences. We have noted that STXM has already made significant contributions to soil biogeochemistry (Lehmann et al. 2005), environmental microbiology (Lawrence et al. 2003; Dynes et al. 2006a,b, 2009), biogeochemistry (Toner et al. 2005), and colloid chemistry (Schumacher et al. 2005; Mitrea et al. 2008), in atmospheric (Braun et al. 2005, 2008), marine/aquatic (Claret et al. 2008; Dynes et al. 2006a, b; Obst et al. 2009a, b), and soil remediation (Yoon et al. 2006).

Carbonaceous airborne particulate matter (CAPM) or soot has considerable deleterious effects on human health and climate; however, it is relatively poorly defined. Braun et al. (2008) applied STXM to characterize subgroups of CAPM, including wood smoke, diesel soot, and urban air. They applied the STXMs at the ALS and NSLS to record *C1s* NEXAFS spectra of single particles of CPM. Their results point to significant differences in diesel exhaust particulates and those of wood smoke; the former have a semi-graphitic solid core, whereas the latter have none or less of this core material. The results help apportion relative contributions of these two air pollutants. This study builds on an earlier STXM study of coal by Cody et al. (1995) and by this same group on diesel exhaust particulates (Braun et al. 2004). Russell et al. (2002) also examined the carbon coatings on atmospheric dust particles.

Another critical issue related to carbonaceous particulate materials is their interaction with hydrophobic organic compounds (HOCs), including PCBs and PAHs in the environment. The sorption of these compounds by carbonaceous particulate materials significantly influences their mobility and bioavailability and our capacity to recover and remediate sites contaminated with PCBs and PAHs. As part of the studies assessing these phenomena, Yoon et al. (2006) applied STXM to assess nanoscale chemical heterogeneities in these carbon materials and how they influence sorption of PCBs. They found that the functional groups of the carbonaceous materials vary on a 25-nm scale corresponding to the abundance of the HOCs. In general these interactions reduce the availability of PCBs in the environment acting to sequester them.

Schumacher et al. (2005) also investigated the chemical heterogeneity of organic colloids at the particle scale, applying STXM spectromicroscopy to 49 individual particles isolated from the surface horizons of three forest soils. They found very large interparticle variation, particularly in the aromatic and carbonyl contents of the particles. Mitrea et al. (2008) used the scanning transmission X-ray microscope at BESSY II to examine colloidal structures from a Chernozem soil at a spatial resolution near 60 nm and a spectral resolution of 1700 at the *C1s* edge to determine the distribution of organic matter in these structures. Natural organic matter also plays an important role in the transport and stability of organic contaminants, and STXM based studies have allowed very fine scale examination of these interactions (Claret et al. 2008).

Dynes et al. (2006a) reported on the use of STXM to examine the spatial distribution of chlorhexidine (1,1′-hexamethylenebis[5-(*p*-chlorophenyl)biguanide]), a widely used antimicrobial agent, in river biofilm communities grown in the presence of 100 μg/L of chlorhexidine digluconate. Similarly, STXM was successfully applied to map the distribution of chlorhexidine in pure bacterial cultures showing its penetration of the cell and accumulation in the lipid fraction of the bacterial cells (Dynes et al. 2009). With STXM, it was possible to show unambiguously that chlorhexidine was sorbed or otherwise chemically associated with the lipids in the diatoms and bacteria. Some of these results are presented in Figures 14.4, 14.6–14.8. It is important to note that attempts to map the ubiquitous environmental contaminant triclosan (see spectra in Fig. 14.7) met with failure as it was not possible to differentiate the contaminant from the complex protein background of the sample; this is an issue in the detection of organic contaminants in many environmental matrices.

Schafer et al. (2007) used a combination of STXM, FTIR, and electron microscopy to study organic colloidal/particulate material sampled as a function of depth in Lake Brienz, an ultraoligotrophic lake in Switzerland. Their study focused especially on organic functionality. Figure 14.9 presents STXM results from a sample at 100 m. The *C1s* spectra clearly show that organic material is associated with potassium rich inorganic colloids present in both the surface and deep water, which indicated a vertical transfer of aggregates by sedimentation. Figure 14.10 presents FTIR microscopy results from the same 100-m-depth sample. There is good correlation of the conclusions reached from both measurements and the NEXAFs and IR spectra of the deep organic matter was very similar to that found in two tributary rivers feeding the lake.

14.2.7. Future Developments in STXM

Although three-dimensional visualization and quantitative analyses are at a reasonably advanced level, there is a need for additional improvements in sample handling, as well as data collection and data analysis. Instrumentation would

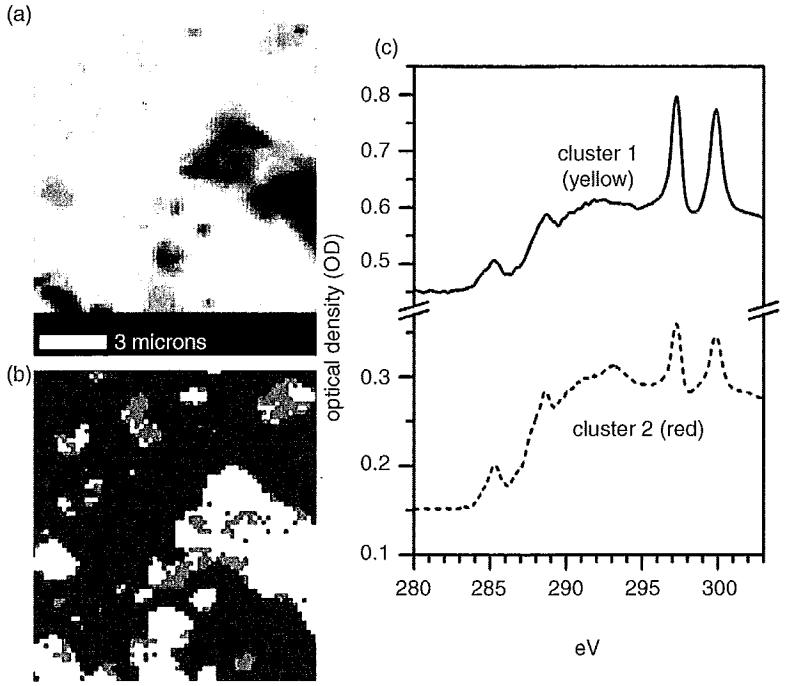

Figure 14.9. STXM analysis of a colloid sample from 100 m below Lake Brienz: (a) absorption image taken at 280 eV below the *C*1*s* edge showing inorganic colloids and particles; (b) PCA and cluster analysis showing distributions of two distinctive clusters (yellow and red) and the background region (blue); (c) corresponding *C*1*s* spectra of yellow and red clusters. [From Schafer et al. (2007), reproduced with permission]. (*See insert for color representation of this figure.*)

benefit from improving resolution to 10 nm, availability of X-ray fluorescence yield detection methods, more rapid raster scanning, improved bright-field detectors, and faster throughput for tomography studies. Many novel experiments could be performed if there were greater control over the sample environment (aerobic, anaerobic, temperature, and capacity to change the environment for experimental purposes). In general, there is a desire or need to obtain conditions as close as possible to the environmental system of interest.

Additional correlative approaches are also being facilitated within the synchrotron research community and with other microspectroscopic and imaging techniques that will allow a much more effective application of these approaches and attendant improvements in our understanding of both the fate and effects of contaminants. However, this will require more attention to sampler holders and navigation to study sites with high precision.

There is also a considerable need for improvements in the postcollection processing and analyses of STXM data stacks to improve both resolution and sensitivity. Different approaches to spectral fitting may allow discrimination between organic contaminants that hitherto were hidden within the predominant backgrounds of organic matter proteins, and other biomolecules.

Three-dimensional visualization is already at a reasonably advanced level. However, new procedures for extraction of quantitative and structural information need to be established in order to automatically analyze multichannel datasets with collocalized signals.

Finally, there remains the challenge of all microscale studies: relating these findings to the much larger scale.

14.2.8. Summary and Conclusions Related to STXM

Soft X-ray scanning transmission X-ray microscopy is both a promising tool for advancing the study of environmental contaminants and one with a high degree of realized promise. Nevertheless, STXM will continue to increase our understanding of processes in the environmental dynamics or organic contaminants. The area of three-dimensional chemical mapping at high spatial resolution using angle scan computed STXM tomography (Johansson et al. 2007; Hitchcock et al. 2008b; Obst et al. 2009b) has great potential with regard to environmental samples. In the near future these approaches likely will increase our understanding of the structures and processes in microbial communities and their role in the fate of environmental contaminants.

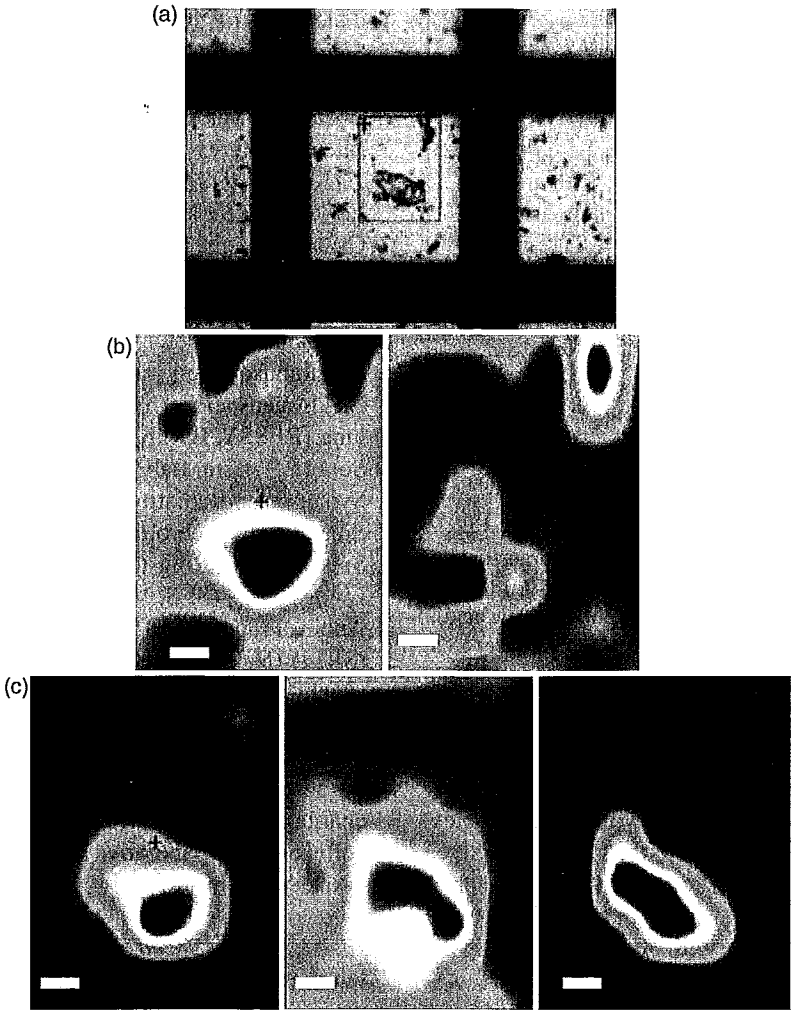

Figure 14.10. FTIR results for a colloid sample from 100 m below Lake Brienz: (a) visual light microscopy image of the TEM grid square subjected to FTIR spectromicroscopy; (b) functional group mappings of aromatics and clay associated OH vibrations at 3620 cm^{-1}; (c) aliphatics as well as correlation maps using target spectra from aquatic organic colloids from tributary rivers (scale bar is = 5 μm) [from Schafer et al. (2007), reproduced with permission].

14.3. SYNCHROTRON-BASED FOURIER TRANSFORM INFRARED MICROSPECTROSCOPY

14.3.1. Infrared Spectroscopy

The infrared part of the electromagnetic spectrum is divided into three regions on the basis of energy: the near (14,000–4000 cm^{-1}), the mid- (4000–400 cm^{-1}) and the far infrared (400-10 cm^{-1}). Far-infrared spectromicroscopy is of interest and, as noted by Miller et al. (2003), has considerable potential, but less is known about the spectra generated and, because of the long wavelength, spatial resolution is very limited (100 μm or worse). The mid-infrared region is the most useful for examining organic contaminants in the environment, so our discussion will focus on this approach. The absorption of midinfrared radiation by molecules excites vibrational modes, which have frequencies determined by atomic masses, bond strengths, and molecular symmetry and structure, and thus are very characteristic of the molecule (Hirschmugl 2002b). Hence, IR spectroscopy can be used to identify functional groups within a molecule (e.g., carboxylic acid), and because each compound has a unique molecular "fingerprint," it can also be used to identify the molecule itself. Indeed, IR spectroscopy is frequently used for the identification of chemical compounds in unknown matrices.

Biochemical molecules such as proteins, lipids, nucleic acids, and carbohyrates have unique IR spectra. For example, proteins have characteristic features labeled *amide I bands* (1600–1700 cm^{-1})—[a carbonyl stretching mode and *amide II bands* (1500–1560 cm^{-1})—a combined N–H bending–

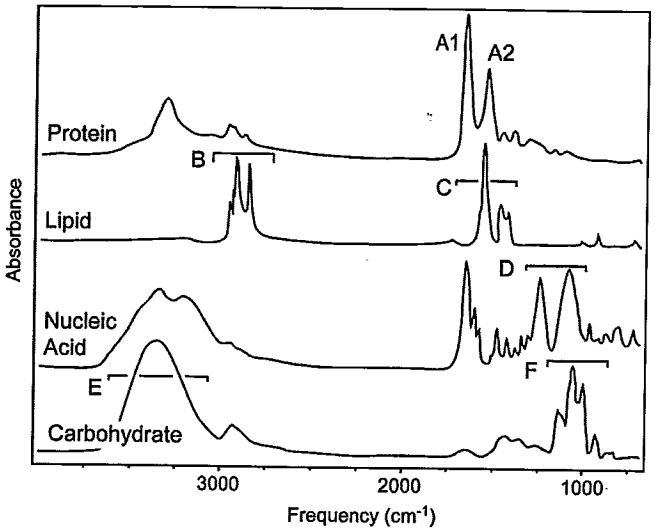

Figure 14.11. Various cellular components have dramatically different IR spectra as demonstrated by IR spectra of (a) a lipid (palmitic acid), (b) a protein (myoglobin), (c) a poly (nucleic acid), and (d) a carbohydrate (sucrose). For all spectra, films were prepared on BaF_2 disks and 128 scans were collected at 4 cm^{-1} resolution using a Globar source. [From Miller et al. (2003), reproduced with permission.]

C–N stretching vibration mode, along with more complex amide III, IV, and further bands. Note that to be IR-active, vibrational modes must involve changes in the permanent dipole moment. Thus, if there are symmetric structures around a site of interest, there will often be little dipole moment, and thus IR will be ineffective in such systems. Stem (2008) provides the following as an example, The ν_{C-H}, the C–H stretching mode, is silent in ethane and has nonactive bonds, but compounds with pendant methyl groups have a strong ν_{C-H} signal (Stem 2008). Figure 14.11 presents the IR spectra for a number of biologically relevant macromolecular species. Infrared microscopy achieves contrast through intramolecular vibrations and the intrinsic IR absorption bands. Jackson and Mantsch (2000) provide an overview of many relevant IR spectra. These spectra can, however, be influenced by sample history, including preparation techniques resulting in significant shifts from expected absorption peaks. [Nevertheless, these shifts can be a rich source of information regarding the sample in question. In addition to qualitative analysis, IR spectroscopy can also be used quantitatively to determine the amount of material present in a sample. (Hirschmugl 2002a,b; Stem 2008).

14.3.1.1. Instrumentation for and Access to FTIR Spectroscopy. Instruments for FTIR spectroscopy, imaging, and spectromicroscopy are commercially available, and they have been implemented at many synchrotron facilities worldwide. Infrared spectromicroscopy facilities in operation or under construction include the National Synchrotron Light Source (NSLS, Brookhaven National Laboratory, USA), the Synchrotron Radiation Center (SRC, University of Wisconsin-Madison, USA), the Center for Advanced Microstructures and Devices (CAMD, Louisiana State University, USA), the Advanced Light Source (ALS, Lawrence Berkeley National Laboratory, USA), the Canadian Light Source (CLS, University of Saskatchewan, Canada), Diamond Light Source (Diamond, Rutherford Appleton Laboratory, UK), Australian Synchrotron (Melbourne, Victoria, Australia), ANKA Synchrotron Strahlunqsquelle (Karlsruhe, Germany), Berliner Elektronenspeicherring-Gesellschaft für Synchrotronstrahlung (BESSY, Berlin, Germany), Elettra Synchrotron Light Source (Trieste, Italy), MAX-lab (Lund, Sweden), National Synchrotron Radiation Center (NSRRC, Hsinchu, Taiwan), Singapore Synchrotron Light Source (SSLS, Singapore), Super Photon Ring (Spring8, Nishi-Harima, Japan), Swiss Light Source (SLS, Villigen, Switzerland), SOLEIL (Saint-Aubin, France), and Synchrotron Light Research Institute (SRLI) (Nakhon Ratchasima, Thailand). A complete list of synchrotrons around the world is available at http://www.als.lbl.gov/als/synchrotron_sources.html. In most cases there is a competitive, peer-reviewed access procedure that regulates the access to IR beamlines. In general, beamline scientists in charge of operations will provide assistance in setup and data collection—collaborative activities are also a common entry point to synchrotron research.

14.3.1.2. IR Spectromicroscopy. Infrared spectrophotometers consist of three main components: the light source, the optical path, and the detector. In the case of synchrotron-based IR, the conventional light source (Globar), is replaced by the high-brightness light emitted by a synchrotron or storage ring, and brought to the microscope and spectrophotometer via a beamline. Relative to Globar radiation, synchrotron IR has lower flux (integrated over all angles), but significantly higher brightness, by a factor of 100–1000 (Duncan and Williams 1983). Thus the main advantage of using synchrotron rather than lab-based FTIR microscopy is seen when the problem under study requires the highest possible spatial resolution. Typically an IR beamline operates under low vacuum ranging from 10^{-3} to 10^{-4} Torr with a diamond window (i.e., 0.5-mm-thick synthetic diamond) isolating the beamline from the high vacuum of the ring. Within the light path starting from the ring itself are a series of mirrors that act to direct the light to the microscope. Mirrors are the functional elements in an IR microscope because of the broad wavelength of IR light and the lack of IR-transparent materials from which to create lenses. The mirrors may be aluminized surfaces. The CLS, BESSY, and ALS the IR beamlines share similar designs and use combinations of planar, ellipsoidal, and cylindrical mirrors to direct the light to a 6-mm-thick KBr, CsI, or polyethylene window.

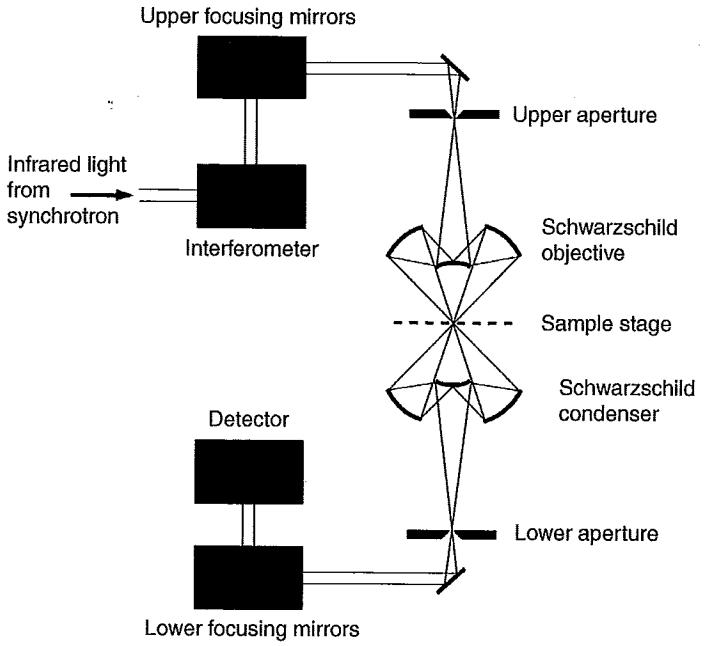

Figure 14.12. Schematic of the Spectra-Tech *Irμs*™ scanning infrared microspectrometer. The system is a combined FTIR spectrometer and microscope, with an upper aperture to define the area being illuminated by the IR, and a lower aperture to limit the detector's field of view onto the sample. The term *confocal* is often used to describe the optical configuration when both apertures are used. [After Miller et al. (2003), reproduced with permission.]

This light is then directed to a spectrometer, and then to piezoelectrically operated mirrors that direct the light through a microscope (May et al. 2007). Since IR light is influenced by water vapor and carbon dioxide, these are most often removed and the microscope is operated under a dry nitrogen or dry air environment. Figure 14.12 illustrates the typical arrangement of an IR beamline set up for FTIR microscopy.

Commercially available IR microscopes from a number of companies (e.g., Thermo Nicolet, Bruker, Bio-Rad, Perkin-Elmer) can be adapted to a synchrotron IR source with very little modification. These microscopes are usually equipped with Schwarzschild objective/condenser pairs for imaging. The objective/condenser pair is arranged in a confocal configuration; one element focuses light on the specimen, while the other collects the light and relays it to the detector. Schwarzschild lenses range in magnification from 6× to 50× and have numerical apertures in the range of 0.3–0.7. In addition, the microscope has upper and lower apertures located between the specimen and the Schwarzschild objective and condenser; these act to limit the area of the specimen illuminated by the beam and the signal being detected. The combination of confocal lenses and apertures results in illumination free of chromatic aberration- and diffraction-limited imaging. The spatial resolution of FTIR spectromicroscopy is diffraction-limited, as it is dependent on the wavelength of light and the numerical aperture of the focusing optic. The aperture controls the region that is illuminated by confining the beam to the sample's area of interest. With a single aperture before the sample, the diffraction-limited spatial resolution is approximately $2\lambda/3$; thus, for the mid-IR range, it is 1.7 μm (at 4000 cm^{-1}) to 13 μm (at 500 cm^{-1}) (Carr 2001; Miller and Dumas, 2006). The addition of the second aperture after the sample further improves the spatial resolution of the microscope by up to $\lambda/2$. Dumas and Miller (2003) describe a conventional synchrotron-based setup for IR microspectroscopy using a Nic-Plan IR microscope coupled to a Magna 560 FTIR spectrometer and a Continuum IR microscope coupled to a Nicolet Magna 860 FTIR spectrometer. As indicated above, a confocal mode was used with a focusing Schwarzschild objective 32× (NA = 0.85) and a collection objective with 10× [numerical aperture (NA) = 0.71] in combination with adjustable upper and lower apertures in the range of $3 \times 3\ \mu m^2$. The reader is referred to the literature for more details on instrument specifics (Smith 1979; Carr 1999; Carr 2001; Miller et al. 2003; Miller and Dumas 2006). The microscopes also provide a range of imaging options allowing the user to observe the sample with differential interference contrast, fluorescence, and polarized light.

Typically the specimen is mounted on a motorized stage allowing the specimen to be moved precisely in the x–y for imaging, and data collection, using a mercury–cadmium–telluride (MCT-A) detector. Mercury–cadmium–telluride

(MCT) arrays [charge-coupled device (CCD) detectors] are available for the infrared region. They may be nitrogen cooled to increase sensitivity and improve the signal to noise ratio of the system (Mills et al. 2005). However, MCT detectors, do have issues with nonlinear response over the full range of brightness. It has been suggested that germanium photoconductor detectors offer a solution to this issue (Miller and Dumas 2006). Miller and Dumas (2006) discuss the application of focal plane array detectors in what is termed *Fourier transform infrared microspectrometry imaging*. In this approach there are an array of IR detectors that allow spectra from various regions of the sample to be collected simultaneously, thereby increasing the speed of collection. In conventional FTIR with a point detector there is either one or two apertures that act to limit the area illuminated and seen by the detector. With a focal plane array (FPA) there are no apertures; thus there is a loss of spatial resolution since the instrument cannot be operated as a confocal microscope. Further details regarding the schematics and operation of a confocal microscope as well as the use of FPA with synchrotron radiation may be obtained from Carr et al. (2005). A multielement detector (IRMSI-MED) for diffraction-limited chemical imaging using parallel acquisition of an array of spectra for microspectroscopic maps has been successfully used at the Synchrotron Radiation Centre (Nasse et al. 2007), greatly increasing the speed of data collection. Quantum structure infrared photodetector (QSIP) technology has been proposed to offer further advantages (LeVan and Beecken 2009).

14.3.1.3. Advantages of Synchrotron IR Source. Conventional light sources for IR spectroscopy have high signal-to-noise ratios (SNRs) that limit their practical resolution to 20 μm; however, this is due to the low intrinsic brightness of Globar sources rather than limitations of the optics of the microscope itself (Dumas and Miller 2003). Indeed, conventional FTIR has a high level of molecular information but lacks the desired spatial resolution, particularly for biological and some environmental applications. A synchrotron IR source is 100–1000 times brighter than a conventional thermal source (Duncan and Williams 1983; May et al. 2007). While a variety of high-brightness sources exist, only synchrotron light provides the full range of wavelengths in the infrared combined with a very small source size and narrow angles of emission (Miller and Dumas 2006). Miller and Tague (2002), state that the use of a high-brightness synchrotron light source dramatically improves spatial resolution, allowing collection of high-quality data at the diffraction limit [3–25 μm in the mid-IR (400–4000 cm^{-1})]. It is important to note, however, that if large aperture settings (> 20 μm) are used, then synchrotron-based IR has no advantage. In the final analysis, the major advantage of synchrotron-based IR spectromicroscopy over many other bioanalytical methods is its ability to distinguish between subtle changes in overall biochemical composition, even in the absence of morphological differences (Jilkine et al. 2008).

14.3.1.4. Sample Preparation. In many cases, depending on the mode of data collection, there is relatively minimal sample preparation, allowing noninvasive in situ types of analyses with IR. However, special requirements may be necessary for transmission, reflection, grazing incidence, attenuated total reflectance, or photoacoustic spectroscopy. If the sample does not transmit adequate light for transmission, lacks reflectivity, or may not allow sufficient penetration of the sample, then special handling may be required.

The most common approach to IR analysis is either transmission or reflectance, although the option exists to carry out a combination of the two methods. Transmission requires thin samples (1–10 μm). In many cases this can be achieved by spotting an appropriate aliquot of material onto an IR transmissive material and drying or maintaining the sample in a fully hydrated state prior to and even during examination. Some type of embedding (paraffin, epoxy, Nanoplast, polymethacrylate) and subsequent sectioning is frequently required. However, cryosectioning is a simpler, less transformative, and generally preferred method of sectioning for many microscopy-based studies. Miller et al. (2003), Miller and Dumas (2006), and Dumas and Miller (2003), in overviews of FTIR and its applications, present a number of sample types and their preparation methods, including bone that was embedded in polymethylmethacrylate and microtomed to 5 μm. The prepared samples were mounted in a compression cell (Thermo Spectra Tech, Shelton, CT) for data collection. They also embedded hair and skin in Tissue Tek (Reichert-Jung, Heidelberg, Germany) and cryosectioned at 5–7 μm. Alzheimer's diseased brain material was snap-frozen in liquid nitrogen, and 15-μm-thick sections were cut with a cryomicrotome and placed on BaF_2 disks. In most instances the prepared materials are placed on an IR transparent window or holder made from ZnS, BaF_2, CaF_2, KBr, ZnSe, or even diamond. Sections prepared for synchrotron IR do not exceed 30 μm in thickness.

In reflection mode prepared sections may also be examined, although they are then mounted on an IR reflective surface such as a low-E glass slide (Kevley Technologies), and the signal collected is that reflected from the support surface after passing through the sample. Since reflection imaging requires extremely smooth surfaces to prevent degradation of the signal, polished sections of mineral, bone, or other materials are well suited to this approach. Miller (2010) provides useful suggestions regarding the mounting of samples on putty or a goniometer to allow optimizing the angle of incidence for reflection analyses of uneven samples. While reflectance is suitable for sections or polished materials at about 10 mm thickness, the application of grazing incidence is best for samples with < 1 mm thickness and

that are highly polished and conducive to high polish such as metals. An additional complication is that grazing incidence requires the use of specially designed Schwartzchild objectives that aid in limiting the penetration of the beam into the surface of material under investigation.

Attenuated total reflection (ATR) infrared spectroscopy uses a high refractive index, infrared-transparent internal reflection element such as Ge, ZnSe, or diamond. This element provides a thin sampling region at its surface where it is in contact with the sample; thus the ATR material has to touch the sample to allow the IR to probe the sample and thereby determine its spectrum. This approach has been used in environmental studies to examine the chemical nature of sorption films by incubating the Ge element in water (Baier 1973), while Geesey and Suci (2000) describe this approach to study biofilms, biocorrosion, and the behavior of molecules at interfaces. Thomasson et al. (2000) described the measurement of IR microspectra utilizing a ATR objective containing a small crystal about 100 μm in diameter. This provided spectroscopic analyses of standard polished thin sections. Certainly there are limitations in terms of sample type, the spectral qualities of the element selected, the need for contact, potential damage to the element, cleaning issues, and so on as noted by Miller (2010). To date ATR does not appear to have been applied with synchrotron radiation but may offer potential. Photoacoustic spectroscopy offers many advantages and requires minimal preparation to obtain spectra for a range of sample types. It does not require transmission, is relatively insensitive to surface conditions of the sample, and can probe a sample with depths from a few micrometers >100 μm (Michaelian 2003). This approach has been applied to a number of solids and liquids, including coal, coke, bitumen, metal powders, wood products, and clays. However, some processing may be required such as grinding or powdering for highly variable samples or solvent extraction and drying as noted by McClelland et al. (2002). Photoacoustic infrared spectroscopy has also been implemented using synchrotron radiation instead of a thermal infrared source (Michaelian 2003; Michaelian et al. 2008).

A number of specific sample preparation approaches that may have particular use for environmentally relevant studies have been outlined by various authors. Jilkine et al. (2008) used low-E microscope slides or gold-coated silicon wafers as substrates for fungal spores which were germinated in humidity chambers. The emerging hyphae grew out across the FTIR slides, and the authors froze and lyophilized the samples before data collection. As in other techniques (see Section 14.2), sulfur embedding and sectioning may be applied to environmental samples to obtain thin sections for FTIR studies (Schafer et al. 2009). Untreated rock samples embedded in sulfur, thin-sectioned (ultramicrotomed to 100 nm thickness) and placed on formvar grids can be used for both STXM and FTIR studies.

Many investigators transfer cultured cells, including human, cancer, *Euglena*, fungi, bacteria to gold-coated surfaces in water or culture media and maintain them in a living hydrated state during timecourses over several days (Hirschmugl 2002a; Dumas and Miller 2003; Holman et al., 2000, 2006; Szeghalmi et al. 2007). Holman et al. (1999), in a classic study, utilized a magnetite surface to carry *Arthrobacter oxydans* cells in a solution containing both chromium and ultimately toluene that was monitored via IR spectromicroscopy for several days. Marinkovic et al. (2000) describe a special flow cell with mixing properties that was specifically designed for FTIR studies. In a more recent study, using high-resolution FTIR, Holman et al. (2009) constructed a special high-humidity chamber to maintain essentially a 1-μm-thick biofilm of *Desulfovibrio vulgaris* and used synchrotron radiation–based Fourier transform infrared (FTIR) spectromicroscopy to determine the cellular chemical environment by continuously monitoring the dynamics of hydrogen bonding in cellular water in vivo. Holman and Martin (2006) refer to the development of automated microfluidic devices that allow manipulation of the microenvironment along with sensors to monitor relevant parameters and allow IR studies of biogeochemical processes in aqueous environments. Fourier transform infrared–compatible humidity cells for live cell visualization that enable real-time biochemical imaging at better than 5 μm spatial resolution are described by Jilkine et al. (2008).

14.3.1.5. Data Collection. Traditionally, infrared beamlines based at synchrotrons use a confocal configuration with raster scanning and a point detection system. However, as noted by a number of authors (Miller and Smith 2005), although the images are of high quality, the collection times are extremely long. While focal plane arrays offer improved collection speed, there are tradeoffs in terms of resolution (see discussion above). Nasse et al. (2007) indicated that a typical microspectroscopic map of 15 × 15 spectra with 128 scans each, at a resolution of 4 cm^{-1} and a mirror velocity of 3.2 cm/s may be acquired in approximately 2.5 h using a point detection system. In contrast, using a multielement detector allows one to obtain chemical images with diffraction-limited resolution of the illuminated area in under a minute (Nasse et al. 2007). When combined with the fact that the intense IR synchrotron infrared beam does not result in heating of the samples and has no effect on living biological systems (Holman et al. 2002b; Martin et al. 2001), this allows real-time analyses and timecourses to be carried out.

The user may start with collection of a reference spectrum in a sample-free area of the specimen holder, such as an IR-reflective slide. Initial observations may be made at larger scale using an aperture open to 30 μm to survey the sample and select regions of interest for detailed mapping and taking specific spectra. Once a region is determined, the aperture

may be reduced to, for example, 12 μm or less for generating IR maps in 10 μm steps along the sample under study.

14.3.1.6. Analysis, Mapping, and Quantification. As is typical in spectromicroscopy, many hundreds of spectra are collected in each measurement, and thus it is a challenge to extract, analyze, and quantify the contained information. There can be considerable difficulty in extracting the signal signature from background/matrix responses in environmental samples, particularly if there is partial absorption saturation. Infrared spectroscopy allows the generation of images representing the chemical composition and distribution occurring with complex environmental samples. Most environmental samples are heterogeneous and complex; therefore, successful analysis, mapping, and quantification are highly dependent on the quality of the spectra acquired, in particular the signal-to-noise ratio, as well as the lateral resolution. Hirschmugl et al. (2006) describe a prescreening of spectra to ensure that intensities are within acceptable limits. Success may also be dependent on providing an effective blank, subtraction of culture medium/liquid water absorbance, or eliminating interferences [i.e., residual water vapor as in the case described by Holman et al. (2009)] and controlling for variations in source strength, due to the fill cycle of most synchrotrons. In this last regard, the recent trend to implementation of so-called top-off modes, where the current in the storage ring is maintained constant within a fraction of a percent, is particularly beneficial to synchrotron-based FTIR microscopy.

Most IR microscopes are equipped with basic analytical packages, although typically these are not sufficient for the task at hand. Additional software is available from suppliers such as Thermo-Nicolet, Bruker, Spectral Dimensions, Cytospec, and Galactic. For example, Holman et al. (2009) performed all data processing with Thermo Electron's Omnic 7.2 (http://www.thermo.com/) and Origin 6.0 (http://www.originlab.com/). Application of Omnic software allows the user a range of options, such as subtraction of the substrate background (IR-reflective glass, etc.), automatic baseline correction, normalization, peak identification, and calculation of peak heights and areas.

In their simplest application, IR spectra are used to evaluate the difference between two measurements in a controlled experiment; in this instance the user is assessing changes in lineshape and strength in a difference spectrum (Hirschmugl 2002a,b). The basic approaches to data analyses have been summarized by Miller (2010) and include the following:

1. Functional group mapping is the most common method for chemical imaging of samples. This is based on measuring peak height, peak area, or the peak height/area ratio. This provides a very basic approach to determining locations and quantity for identifiable compounds.
2. Second derivatives and Fourier self-deconvolution are used to identify peak frequencies.
3. Correlation methods are used to compare standard spectra to unknowns obtained from the sample wherein a perfect match has $r = 1.0$.
4. Cluster analyses, which employ statistical methods, are used to evaluate spectral similarity in order to group spectra that may then be extracted or averaged and interpreted relative to known spectra.

Spectral analyses may also benefit from the application of multivariate statistical analysis techniques such as linear discriminate and principal-component analyses (PCAs). The applications of cluster and PCA data treatments are driven in large measure by the collection of spatial datasets. For example, Schafer et al. (2009) applied both PCA and cluster analysis. Their results showed that humic acids were best correlated with organics found in smectite-rich regions, while fulvic acids grouped with the organics found in the illite mixed-layer materials. Hirschmugl et al. (2006) describe the application of agglomerative hierarchical clustering to FTIR datasets. This required prescreening, and conversion to first derivatives using a Savitzky–Golay algorithm, followed by normalization so that the sum-squared deviation equaled unity. The resulting cluster analysis calculates a distance matrix of the similarity of the spectra and uses these data to produce a dendrogram wherein the spectral sets are grouped according to their similarity. This allowed discrimination of *Euglena gracilis* cells on the basis of their nutritional history. Similarly, Yu (2007) found that they could use IR spectra and agglomerative hierarchical cluster analysis to distinguish inherent differences between maize and barley feed quality, as well as detecting the aleurone (protein, starch) and pericarp (lignin, cellulose) structural layers of seeds. Artificial neural network (ANN) methods are also being applied. General information on these methods may be obtained from a number of references (Jackson and Mantsch 1999; Naumann 2002; Chalmers and Griffiths 2002). It is felt that statistical pattern recognition techniques offer a simpler and unbiased approach to analyses of large spectral datasets (Hirschmugl et al. 2006; Lasch and Naumann 1988) relative to fitting or inspection techniques.

Chemical maps are created from spectra by determining the intensity of an absorption band at each measuring position such that different bands create different maps. The peak height in the absorption spectra is proportional to the concentration of that functional group at a specific location. The user may obtain a quantitative impression of the map if object thickness can be obtained for each x–y location or by using a ratio method between peaks. Each peak or band may be assigned to a functional group. Timecourses may also be obtained with IR microspectroscopy to allow assessment of

changes with treatment or exposure, see for example (Holman et al. 2009) who created time-difference spectra using Thermo Electron's Omnic 7.2 software (http://www.thermo.com/)] from experimental spectra after subtraction of culture medium/liquid water absorbance.

14.3.2. Examples of the Application of IR Microspectroscopy

Although there are a variety of "environmental" applications of synchrotron-based infrared microspectroscopy, the series of publications by Holman in conjunction with various authors. (Several articles by Holman et al. 1997, 1998a,b, 1999, 2002a,b, 2009) represent an excellent series of examples. These studies illustrate the use of incubation methods and variations of the synchrotron-based IR approach to investigate inorganic–organic interactions at bacterial–mineral interfaces, localization of bacteria on geologic surfaces, evaluation of the effects of changing humidity on microbial activity, biogeochemical reduction of Cr(VI) on basalt surfaces, and catalysis of PAH biodegradation by humic acids. In addition to the development of the technique, these publications are also basic studies generating important insights into biogeochemical processes.

14.3.2.1. Real-Time Characterization of Biogeochemical Reduction of Cr(VI) on Basalt Surfaces by SR-FTIR Imaging. Holman et al. (1999) provide an excellent example of applying IR synchrotron imaging to monitor the reduction of Cr(VI) (oxidation state of Cr(III) compounds and the metabolism of toluene by bacterial colonies on a basalt surface, providing results on the oxidation state of Cr that were confirmed by micro-X-ray absorption fine-structure spectroscopy. Fourier transform IR spectromicroscopy was carried out on a model surface, magnetite, with the organism *Arthrobacter oxydans*, with and without toluene vapour as a carbon source and cocontaminant. Their biomass determinations and collocalization studies showed that endolithic bacteria were necessary to achieve a reduction of Cr(VI) to Cr(III) and that the presence of toluene as a carbon source enhanced the process. They observed a decrease in the concentration of the organic molecules at the same location as the living cells that were mapped relative to the toluene, based on the detection of amide absorption maxima (Holman et al. 1999). Although cell- or microcolony-level resolution remains an issue, this study demonstrated the capacity of IR microscopy to identify and quantitate molecules, including the mapping of metals, biological macromolecules, and chlorinated chemicals in a biofilm.

In a related study, Holman et al. (2002a) used IR spectromicroscopy to examine the role of humic acids in the biodegradation of polycyclic aromatic hydrocarbons (PAHs) by a *Mycobacterium* species. The bacterium was grown on magnetite surfaces in a specially constructed stage-mounted miniatureincubator. To initiate the experiments, they exposed the inoculated magnetite surfaces to pyrene, which sorbed and diffused into the magnetite. In some cases 300 ppm of filter-sterilized humic acid was applied on top of the pyrene. The degradation of pyrene was monitored in situ over time by returning to a series of selected sample locations and collecting a time series of spectra. Humic acid dramatically shortened the onset of pyrene biodegradation from 168 to 2 h. There was an increase in biomass absorption during the latter stage of pyrene degradation, implying that biomass formation was concurrent with the consumption of pyrene. The role of HA is to speed up the solubilization of the pyrene, making it bioavailable for degradation. It appears that the water-insoluble pyrene is solubilized into the cores of HA pseudomicelles, thereby becoming directly available for bacterial uptake and consumption. Figure 14.13 illustrates the results obtained by IR mapping obtained at the end of the experiment with IR absorption peaks corresponding to the *Mycobacterium* sp., elliott soil humic acid (ESHA) and pyrene. The images show a region with a high density of bacteria and ESHA at locations where pyrene has been degraded by the bacteria. The study demonstrated that nontoxic humic acid may be a useful alternative to other surfactants in enhancing in situ remediation of poorly soluble contaminants. From the perspective of synchrotron-based FTIR microspectrometry, this study demonstrated the capacity to monitor a number of factors in real time under in situ conditions without damage from the IR data collection. However, there are also clear limitations in that only highly selected areas, that is areas that are very flat and within the focal limits, could be included in the monitoring, and the maps produced had 5 μm resolution.

14.3.2.2. Synchrotron Fourier Transform IR Microspectroscopy: A New Tool for Monitoring the Fate of Organic Contaminants in Plants. Phytoremediation is a process wherein plants absorb and biodegrade antheopogenic pollutants from contaminated soil. Dokken et al. (2005a) explored the use of IR spectromicroscopy to examine the fate of contaminant directly in plant material. The authors used FTIR spectromicroscopy to monitor the fate and effects of 2,6-dinotrotoluene (2,6-DNT) in corn (*Zea mays*) roots. Seedlings were grown hydroponically and exposed to 0, 5, 10, and 15 mg/L of 2,6-dinotrotoluene. Root material was frozen in Tissue-Tek OCT (Sakura Finetek USA, Inc., Torrance, CA) at −40°C, and 4-μm sections were prepared and mounted on IR reflecting low-E glass microscope slides. The IR imaging indicated that 2, 6-DNT may be incorporated in the lignin in corn plants. The detection of the nitro peak at 1530 cm^{-1}, CH_3 peaks, and bands typical of aromatic ring structures are indicative of a lack of transformation of the 2,6-DNT prior to incorporation.

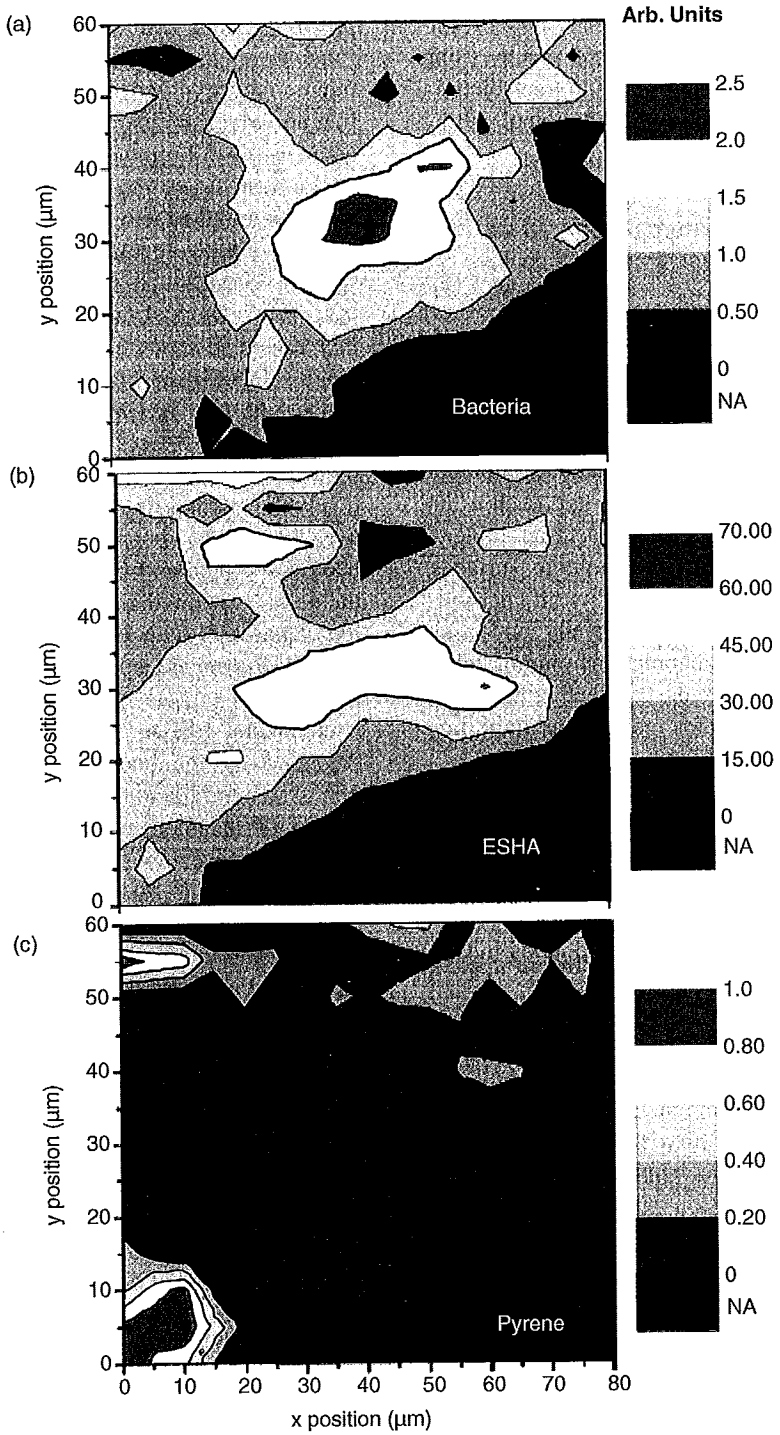

Figure 14.13. Contour diagrams from infrared mapping obtained at the end of the experiment showing the spatial distribution of the infrared absorption peaks corresponding to (a) *Mycobacterium* sp. JLS bacteria, (b) elliott soil humic acid (ESHA), and (c) pyrene. Appropriate spectral regions were integrated for each point on the maps. The color scales for each contour plot are red for highly integrated IR peak area (high concentration of the corresponding component) and blue for low peak area (low concentration); black is an out-of-focus region of the sample. The center of the map shows a region with high density of bacteria and high concentration of ESHA where pyrene has been completely degraded. [Reprinted from Holman et al. (2002a).] (*See insert for color representation of this figure.*)

Similar results were obtained for ^{1}H-benzotriazole in the root tips of sunflowers. Here spectral analyses using principal component methods again suggested that the aromatic ring structure remained intact during absorption, transport and sequestration in plant tissues (Dokken et al. 2005b). Given that modifications to the surrounding plant tissue could also be monitored, this approach was concluded to be a useful option for direct detection of the fate and effects of contaminants in plant tissues.

14.3.2.3. Organic Matter Stabilization in Soil Microaggregates: Implications from Spatial Heterogeneity of Organic Carbon Contents and Carbon Forms. Lehman et al. (2005) used a combination of FTIR and STXM (NEXAFS) microscopies to map the distribution of carbon and its chemical forms in intact soil microaggregates (20–250 mm). The microaggregates were saturated with water, frozen, and sectioned (300–600 nm thickness) without embedding before being placed on copper grids and air-dried. Then STXM analyses were carried out using the Stony Brook STXM at NSLS BL X1A at Brookhaven National Laboratory by collecting stacks between 280 and 310 eV at increments varying between 0.3 and 0.1 eV. The authors then used these stacks to map the carbon amounts in the aggregate sections. Fourier transform IR was also carried out at the NSLS on the U108 beamline using the Spectra Tech Continuum IR microscope with a mercury–cadmium–telluride detector with 500–4000 cm^{-1} wavenumber range and 1.0 cm^{-1} spectral resolution. Mapping was carried out with a 7 mm aperture and a step size of 6 mm or 4000–650 cm^{-1} at intervals of 4 cm^{-1}; 256 scans were added prior to Fourier transformation. They then assessed the spectra for peaks corresponding to stretching vibrations indicative of kaolinite, aliphatic biopolymers, aromatic carbon, and polysaccharides. This allowed them to examine the distribution of total carbon as well as the specific carbon forms in these microaggregates. Although the distribution of carbon based on *C1s* NEXAFS at 0.05 μm resolution appeared random, the types of carbon mapped using FTIR spectromicroscopy mapped at 5 μm resolution exhibited spatial patterns. Although the authors applied this approach to determine the developmental patterns and stabilization of soil aggregates, it could be easily extended to include mapping of associated metals, or organic contaminants providing information important to fate, effects and remediation schemes.

Fourier transform IR spectromicroscopy also has tremendous potential in the field of toxicology, where it has seen direct applications, as well as studies suggestive of this use. See, for example, Holman et al. (2002b), who demonstrated the use of synchrotron IR spectromicroscopy to examine individual living cells. Holman et al. (2000) applied this approach to examine the response of single cells to a toxic organic contaminant Jilkine et al. (2008) used FTIR spectromicroscopy to study differences between optimal and mildly stressed fungi (pH 5.0–8.5), while Szeghalmi et al. (2007) detected subcellular changes accompanying thermal stress in a variety of fungi. In this latter case the authors used specific gene mutations. They noted that FTIR spectromicroscopy facilitated interpretation of the biochemical effect of the gene in the context of the fungal hyphae. In a related study Hirschmugl et al. (2006) were able to spatially resolve the green flagellate *Euglena gracilis* and collect complete spectra for individual cells, which allowed them to discriminate cells on the basis of their nutritional status. Earlier studies had demonstrated the efficacy of FTIR spectromicroscopy in studying the biochemical composition of algae (Giordano et al. 2001).

Fourier transform infrared has also proved useful in the characterization of wax deposits formed in oil-producing wells. Comparison of spectra from nonpolar and predominantly polar aggregates indicated that the polar aggregates contain higher relative concentrations of an inorganic material, most likely $CaCO_3$ (Marinkovic et al. 2002).

14.3.3. Future Developments in Synchrotron-Based FTIR Microscopy

Lombi and Susini (2009) provide a fairly exhaustive review of the literature relevant in the main to X-ray microscopy techniques, including STXM, but also with reference to FTIR and other synchrotron-based techniques. In addition, they consider future directions and required developments quite extensively. In general, it is anticipated that there will continue to be considerable improvement in optics, detectors, and software related to FTIR spectromicroscopy and other synchrotron techniques, including STXM. New beamlines and microscopes are able to provide improved signal-to-noise ratios and increased spatial resolution, as well as improved acquisition times allowing real-time imaging of biological and biogeochemical processes of interest to environmental sciences. Developments such as the ID21 beamline at the ESRF, which is a combination of STXM and FTIR microscopes, is an excellent step in the necessary process of integrating FTIR with other synchrotron-based microspectrometric techniques (Lombi and Susini 2009; Dumas and Miller 2003). In addition to technical developments in beamlines and microscopes, further developments in sample handling and preparation as well as functional model systems and incubation systems are required. Another trend is that of integration of synchrotron analytical microscopies with genomic and other emerging experimental and analytical approaches. Owing to the inherent interdisciplinary nature of environmental science, only a combination of different techniques will provide a complete picture of environmental processes.

14.3.4. Summary and Conclusions Related to Synchrotron-Based FTIR Microscopy

Fourier transform infrared spectroscopy (FTIR) is an analytical technique that allows examination of a variety of sample types, including solids, liquids, gases, and their mixtures. In addition, FTIR facilitates the analyses of a wide range of biological materials providing structural and chemical analyses. The method allows identification of most organic compounds. Indeed, outside of magnetic resonance techniques, FTIR is perhaps the most powerful tool for identifying types of chemical bonds. State-of-the-art FTIR spectromicroscopy in the mid-IR region (0.01–1 eV) allows the production of 2D spectral maps of IR absorption, with a spatial resolution on the order of a few micrometers. Analysis of the absorption signatures permits identification and mapping of the chemical compounds present. Infrared spectroscopy is especially sensitive to vibrations of polar bonds such as O–H, C–H, C–O, N–H, and C–N. Fourier transform IR spectromicroscopy can identify and quantitatively map molecules such as metals, biological macromolecules, and chlorinated chemicals, in environmental samples. Infrared spectroscopy is able to detect subtle biochemical and biogeochemical changes within a range of environmental samples and is able to deal with the relatively high heterogeneity present in environmentally relevant materials and model systems. However, the spatial resolution remains limited. Developments since circa 1990, particularly the use of synchrotron radiation, as a high brightness, full spectral source, have revolutionized FTIR and X-ray spectromicroscopy, creating techniques suitable for high-resolution imaging and spectroscopy and powerful research tools for studying organic contaminants in the environment.

REFERENCES

Ade, H. (1998), X-ray spectromicroscopy, in *Experimental Methods in the Physical Sciences*, Vol. 32, Samson, J. A. R. and Ederer, D. L., eds., Academic Press, New York, pp. 225–262.

Ade, H. and Urquhart, S. G. (2002), NEXAFS spectroscopy and microscopy of natural and synthetic polymers, in *Chemical Applications of Synchrotron Radiation*, Sham, T. K. ed., World Scientific Publishing, Singapore, pp. 285–355.

Ade, H. and Hitchcock, A. P. (2008), NEXAFS microscopy and resonant scattering: Composition and orientation probed in real and reciprocal space, *Polymer* **49**, 643–675.

Baier, R. E. (1973), Influence of the initial surface condition of materials on bioadhesion, in Acker, R. F. ed., *Proc. 3rd Int. Congress Marine Corrosion and Fouling*, Northwestern University Press, Evanston, IL, pp. 633–639.

Bertsch, P. M. and Hunter, D. B. (2001), Applications of synchrotron-based X-ray microprobes, *Chem. Rev.* **101**(6), 1809–1842.

Bluhm, H., Andersson, K., Araki, T., Benzerara, K., Brown, G. E., Dynes, J. J., Ghosal, S., Gilles, M. K., Hansen, H.-Ch., Hemminger, J. C., Hitchcock, A. P., Ketteler, G., Kilcoyne, A. L. D., Kneedler, E., Lawrence, J. R., Leppard, G. G., Majzlam, J., Mun, B. S., Myneni, S. C. B., Nilsson, A., Ogasawara, H., Ogletree, D. F., Pecher, K., Salmeron, M., Shuh, D. K., Tonner, B., Tyliszczak, T., Warwick, T., and Yoon, T. H. (2005), Soft X-ray microscopy and spectroscopy at the molecular environmental science beamline at the advanced light source, *J. Electron. Spectrosc. Relat. Phenom.* **150**, 86–104.

Bradley, J. P., Keller, L., Thomas, K. L., Vander Wood, T. B., and Brownlee, D. E. (1993), Carbon analyses of IDPs sectioned in sulfur and supported on beryllium films (abstract), *Proc. 24th Lunar and Planetary Science Conf.* p. 173.

Braun, A. (2005), Carbon speciation in airborne particulate matter with C (1s) NEXAFS spectroscopy, *J. Environ. Monit.* **7**, 1059–1065.

Braun, A., Huggins, F. E., Kubátová, A., Wirick, S., Maricq, M. M., Mun, B. S., McDonald, J. D., Kelly, K. E., Shah, N., and Huffman, G. P. (2008), Toward distinguishing woodsmoke and diesel exhaust in ambient particulate matter, *Environ. Sci. Technol.* **42**, 374–380.

Braun, A., Shah, N., Huggins, F. E., Huffman, G. P., Wirick, S., Jacobsen, C., Kelly, K. E., and Sarofim, A. (2004), Study of fine diesel particulate matter with scanning transmission X-ray spectroscopy, *Fuel* **10**(7/8), 997–1000.

Brown, G. E. Jr. and Sturchio, N. C. (2002), An overview of synchrotron radiation applications to low temperature geochemistry and environmental science, in *Applications of Synchrotron Radiation in Low-Temperature Geochemistry and Environmental Science*, Fenter, P., Rivers, M., Sturchio, N. C., and Sutton, S. eds., Reviews in Mineralogy and Geochemistry (series) Vol. 49, Geochemical Society, pp. 149–220.

Carr, G. L. (2001), Resolution limits for infrared microscopy explored with synchrotron radiation, *Rev. Sci. Instrum.* **72**, 1613–1619.

Carr, G. L. (1999), High-resolution microspectroscopy and subnanosecond time-resolved spectroscopy with the synchrotron infrared source, *Vlb. Spectrosc.* **19**, 53–60.

Carr, G. L., Chubar, O., and Dumas P. (2005), Multichannel detection with a synchrotron light source: Design and potential, in *Spectrochemical Analysis Using Infrared Multichannel Detectors*, Bhargava, R. and Levin, I. eds., Blackwell Publishing, pp. 56–83.

Chalmers, J. M. and Griffiths, P. R. (2002), *Handbook of Vibrational Spectroscopy*, Wiley, Hoboken, NJ.

Claret, F., Schäfer, T., Brevet, J., and Reiller, P. E. (2008), Fractionation of Suwannee River fulvic acid and Aldrich humic acid on alpha-Al_2O_3: Spectroscopic evidence, *Environ. Sci. Technol.* **42**, 8809–8815.

Cody, G. D, Brandes, J., Jacobsen, C., and Wirick, S. (2009), Soft X-ray induced chemical modification of polysaccharides in vascular plant cell walls, *J. Electron Spectrosc. Relat. Phenom.* **170**, 57–64.

Cody, G. D., Botto, R. E., Ade, H., Behal, S., Disko, M., and Wirick, S. (1995), Microanalysis and scanning X-ray microscopy of

microheterogeneities in a high-volatile bituminous coal, *Energy Fuels* **9**, 75–83.

Dokken, K. M., Davis, L. C., and Marinkovic, N. S. (2005a), Using SR-IMS to study the fate and transport of organic contaminants in plants, *Spectroscopy* **20**, 14–20.

Dokken, K. M., Davis, L. C., Erickson, L. E., Castro-Diaz, S., and Marinkovic, N. S. (2005b), Synchrotron Fourier transform infrared microspectroscopy: A new tool to monitor the fate of organic contaminants in plants, *Microchem. J.* **81**, 86–91.

Dumas, P. and Miller, L. M. (2003), The use of synchrotron infrared microspectroscopy in biological and biomedical investigations, *Vibrat. Spectrosc.* **32**, 3–21.

Duncan, W. and Williams, G. P. (1983), Infrared synchrotron radiation from electron storage rings, *Appl. Opt.* **22**, 2914–2923.

Dynes, J. J., Lawrence, J. R., Korber, D. R., Swerhone, G. D. W., Leppard, G. G., and Hitchcock, A. P. (2006a), Quantitative mapping of chlorhexidine in natural river biofilms, *Sci. Total Environ.* **369**, 369–383.

Dynes, J. J., Tyliszczak, T., Araki, T, Lawrence, J. R., Swerhone, G. D. W., Leppard, G. G., and Hitchcock, A. P. (2006b), Quantitative mapping of metal species in bacterial biofilms using scanning transmission X-ray microscopy, *Environ. Sci. Technol.* **40**, 1556–1565.

Dynes, J. J., Lawrence, J. R., Obst, M., Swerhone, G. D. W., Korber, D. R., Leppard, G. G., Tyliszczak, T., and Hitchcock, A. P. (2009), Soft X-ray spectromicroscopy of nickel sorption in a natural river biofilm, *Geobiology* **7**, 432–453.

Feser, M., Beetz, T., Carlucci-Dayton, M., and Jacobsen, C. (2000), Instrumentation advances and detector development with the Stony Brook scanning transmission X-ray microscope, *AIP Conf. Proc.* **507**, 367–372.

Geesey, G. G. and Suci, P. A. (2000), Monitoring biofilms by Fourier transform infrared spectroscopy, in *Biofilms: Recent Advances in Their Study and Control*, Evans, L.V. ed., Harwood Academic Publishers, Chur, Switzerland, pp. 253–277.

Gilbert, E. S., Khlebnikov, A., Meyer-Ilse, W. and Keasling, J. D. (1999), Use of soft X-ray microscopy for the analysis of early-stage biofilm formation, *Water Sci. Technol.* **39**, 269–272.

Giordano, M., Kansiz, M., Haeraud, R., Beardall, J., Wood, B., and McNaughton, D. (2001), Fourier transform infrared spectroscopy as a novel tool to investigate changes in intracellular macromolecular pools in the marine microalgae *Chaetorceros muellerii* (Bacillariophyceae), *J. Phycol.* **37**, 271–279.

Gu, W. W., Etkin, L. D., Le Gros, M. A., and Larabell, C. A. (2007), X-ray tomography of Schizosaccharomyces pombe, *Differentiation* **75**, 529–535.

Henke, B. L., Gullikson, E. M., and Davis, J. C. (1993), At Data Nucl Data Tables, **54**, 181–297.

Hirschmugl, C. J. (2002a), Applications of storage ring infrared spectromicroscopy and reflection-absorption spectroscopy to geochemistry and environmental science, *Rev. Miner. Geochem.* **49**, 317–339.

Hirschmugl, C. J. (2002b), Frontiers in infrared spectroscopy at surfaces and interfaces, *Surf. Sci.* **500**, 577–604.

Hirschmugl, C. J., Bayarri, Z.-E, Bunta, M., Holt, J. B., and Giordano, M. (2006), Analysis of the nutritional status of algae by Fourier transform infrared chemical imaging, *Infrared Phys. Technol.* **49**, 57–63.

Hitchcock, A. P., Araki, T., Ikeura-Sekiguchi, H., Iwata, N., and Tani, K. (2003), 3d chemical mapping of toners by serial section scanning transmission X-ray microscopy, *J. Phys. IV France* **104**, 509–512.

Hitchcock, A. P., Dynes, J. J., Johansson, G. A., Wang, J., and Botton, G. (2008a), Comparison of NEXAFS microscopy and TEM-EELS for studies of soft matter, *Micron* **39**, 741–748.

Hitchcock, A. P., Johansson, G. A., Mitchell, G. E., Keefe, M., and Tyliszcak, T. (2008b) , 3D chemical imaging using angle-scan tomography in a soft X-ray scanning transmission X-ray microscope, *Appl. Phys. A* **92**, 447–452.

Hitchcock, A. P., Morin, C., Zhang, X., Araki, T., Dynes, J. J., Stöver, H., Brash, J. L., Lawrence, J. R., and Leppard, G. G. (2005), Soft X-ray spectromicroscopy of biological and synthetic polymer systems, *J. Electron Spectrosc. Relat. Phenom.* **144–147** 259–269.

Hitchcock, A. P. (2009), *aXis2000 Is an IDL-Based Analytical Package;* available at http://unicorn.mcmaster.ca/aXis2000.html.

Hitchcock, A. P., Morin, C., Heng, Y. M., Cornelius, R. M., and Brash, J. L. (2002), Towards practical soft X-ray spectromicroscopy of biomaterials, *J. Biomater. Sci. Polym. Educ.* **13**, 919–938.

Holman, H.-Y. N., Perry, D. L., and Hunter-Cevera, J. C. (1997), Use of infrared microspectroscopy to assess effects of relative humidity on microbial population and their activity in fractured rocks, *Proc. Gordon Conf. Applied Environmental Microbiology*, Aug. 17–22 1997.

Holman, H.-Y. N., Perry, D. L., and Hunter-Cevera, J. C. (1998a), Surface-enhanced infrared absorption reflectance SEIRA.microspectroscopy for bacteria localization on geologic material surfaces, *J. Microbiol. Meth.* **34**, 59–71.

Holman, H.-Y. N., Perry, D. L., Martin, M. C., Lamble, G. M., McKinney, W. R., and Hunter-Cevera, J. C. (1999), Real time characterization of biogeochemical reduction of Cr VI.on basalt surfaces by SR-FTIR imaging, *Geomicrobiol. J.* **16**, 307–323.

Holman, H.-Y. N., Perry, D. L., Martin, M. C., and McKinney, W. R. (1998b), Applications of synchrotron infrared microspectroscopy to the study of inorganic–organic interactions at the bacterial–mineral interface, *Appl. Synchrotron Radiat. Tech. Mater. Sci. MRS Symp. Ser.* **54**, 17–24.

Holman, H.-Y. N. and Martin, M. C. (2006), Synchrotron radiation infrared spectromicroscopy: A non-invasive molecular probe for biogeochemical processes, *Adv. Agron.* **90**, 79–127.

Holman, H.-Y. N., Nieman, K., Sorensen, D. L., Miller, C. D., Martin, M. C., Borch, T., Mckinney W. R., and Sims, R. C. (2002a), Catalysis of PAH biodegradation by humic acid shown in synchrotron infrared studies, *Environ. Sci. Technol.* **36**, 1276–1280.

Holman, H.-Y. N., Bjornstad, K. A., McNamara, M. P., Martin, M. C., McKinney, W. R., and Blakely, E. A. (2002b), Synchrotron infrared spectromicroscopy as a novel bioanalytical microprobe

for individual living cells: Cytotoxicity considerations, *J. Biomed. Opt.* **7**, 417–424.

Holman, H.-Y. N., Goth-Goldstein, R., Martin, M. C., Russell, M. L., and McKinney, W. R. (2000), Low-dose responses to 2,3,7,8-tetrachlorodibenzo-p-dioxin in single living human cells measured by synchrotron infrared spectromicroscopy, *Environ. Sci. Technol.* **34**, 2513–2517.

Holman, H-Y. N., Wozei, E., Lin, Z., Comolli, L. R., Ball, D. A., Borglin, S., Fields, M. W., Hazen. T. C., and Downing, K. H. (2009), Real-time molecular monitoring of chemical environment in obligate anaerobes during oxygen adaptive response. Proceedings of the National Academy of Sciences of the United States of America, **106**(31),12599–12604.

Howells, M., Jacobsen, C., and Warwick, T. (2007), Principles and applications of zone plate X-ray microscopes, in *The Science of Microscopy*, Hawkes, P. and Spence, J. eds., Kluwer Press, pp. 835–926.

Hunter, R. C., Hitchcock, A. P., Dynes, J. J., Obst, M., and Beveridge, T. J. (2008), Mapping the speciation of iron minerals in *Pseudomonas aeruginosa* biofilms using scanning transmission x-ray microscopy, *Environ. Sci. Technol.* **42**, 8766–8772.

Jackson, M. and Mantsch, H. H. (1999), Ex vivo tissue analysis by infrared microspectroscopy, in *Handbook of Vibrational Spectroscopy,* Chalmers, J. and Griffiths, P., eds., Wiley, New York.

Jackson, M. and Mantsch, H. H. (2000), *Encyclopedia of Analytical Chemistry*, Wiley, Chichester, UK.

Jacobsen, C. (2009), Analysis software and manuals; available at http://xray1.physics.sunysb.edu/.

Jacobsen, C., Feser, M., Lerotic, M., Vogt, S., Maser, J., and T. Schäfer. (2003), Cluster analysis of soft x-ray spectromicroscopy data, *J. Phys. IV* **104**, 623–626.

Jacobsen, C., Kirz, J., and Williams, S. (1992), Resolution in soft X-ray microscopes, *Ultramicroscopy*, **47** 55–79.

Jacobsen, C., Wirick, S., Flynn, G., and Zimba, C. (2000), Soft X-ray spectroscopy from image sequences with sub-100 nm spatial resolution, *J. Microsc.* **197**, 173–184.

Jacobsen, C., Williams, S., Anderson, E., Browne, M. T., Buckley, C. J., Kern, D., Kirz, J., Rivers, M., and Zhang, X. (1991), Diffraction-limited imaging in a scanning transmission x-ray microscope, *Optics Communications*, **86**, 351–364.

Jilkine, K., Gough, K. M., Julian, R., and Kaminskyj, S. G. W. (2008), A sensitive method for examining whole-cell biochemical composition in single cells of filamentous fungi using synchrotron FTIR spectromicroscopy, *J. Inorg. Biochem.* **102**, 540–546.

Johansson, G. A., Dynes, J. J., Hitchcock, A. P., Tyliszczak, T., Swerhone, G. D. W., and Lawrence, J. R. (2006), Chemically sensitive 3D imaging at sub 100 nm spatial resolution using tomography in a scanning transmission x-ray microscope, in *Developments in X-Ray Tomography V*, Bonse, U. ed., *Proc. SPIE*, 6318, 11.

Johansson, G. A., Tyliszczak, T., Mitchell, G. E., Keefe, M., and Hitchcock, A. P. (2007), Three dimensional chemical mapping by scanning transmission X-ray spectromicroscopy, *J. Synchrotron Radiat.* **14**, 395–412.

Kilcoyne, A. L. D., Steele, W. F., Fakra, S, Hitchcock, P., Franck, K., Anderson, E., Harteneck, B., Rightor, E. G., Mitchell, G. E., Hitchcock, A. P., Yang, L., Warwick, T., and Ade, H. (2003), Interferometrically controlled scanning transmission microscopes at the Advanced Light Source, *J. Synchrotron Radiat.* **10**, 125–136.

Kinyangi, J., Solomon, D., Liang, B., Lerotic, M., Wirick, S., and Lehmann, J. (2006), Nanoscale biogeocomplexity of the organomineral assemblage in soil: Application of STXM microscopy and C 1s-NEXAFS spectroscopy, *Soil Sci. Soc. Am. J.* **70**, 1708–1718.

Kirz, J., Jacobsen, C., and Howells, M. (1995), Soft X-ray microscopes and their biological applications, *Q. Rev. Biophys.* **28**, 33–130.

Kirz, J. and Rarback, H. (1985), Soft X-ray microscopes, *Rev. Sci. Instrum.* **56**, 1–13.

Koprinarov, I. N., Hitchcock, A. P., McCrory, C., and Childs, R. F. (2002), Quantitative mapping of structured polymeric systems using singular value decomposition analysis of soft X-ray images, *J. Phys. Chem. B* **106**, 5358–5364.

Koprinarov, I. N., Hitchcock, A. P., Li, W. H., Heng, Y. M., and Stöver, H. D. H. (2001), Quantitative compositional mapping of core-shell polymer microspheres by soft X-ray spectromicroscopy, *Macromolecules* **34**, 4424–4429.

Larabell, C. A. and Le Gros, M. A. (2004), X-ray tomography generates 3D reconstructions of the yeast, *Saccharomyces cerevisiae,* at 60-nm resolution, *Molec. Biol. Cell* **15**, 957–962.

Lasch, P. and Naumann, D. (1988), FT-IR microspectroscopic imaging of human carcinoma thin sections based on pattern recognition techniques, *Cell. Molec. Biol.* **44**, 189–202.

Lawrence, J. R, Swerhone, G. D. W., Leppard, G. G., Araki, T., Zhang, X., West, M. M., and Hitchcock, A. P. (2003), Scanning transmission x-ray, laser scanning and transmission electron microscopy mapping of the exopolymeric matrix of microbial biofilms, *Appl. Environ. Microbiol.* **69**, 5543–5554.

Lehmann, J., Liang, B., Solomon, D., Lerotic, M., Luizao, F., Kinyangi, J., Schafer, T., Wirick, S., and Jacobsen, C. (2005), Near-edge X-ray absorption fine structure (NEXAFS) spectroscopy for mapping nano-scale distribution of organic carbon forms in soil: Application to black carbon particles, *Global Biogeochem. Cycles* **19**, 1013–1025.

Lerotic, M., Jacobsen, C., Gillow, J. B., Francis, A. J., Wirick, S., Vogt, S., and Maser, J. (2005), Cluster analysis in soft X-ray spectromicroscopy: Finding the patterns in complex specimens, *J. Electron Spectrosc. Relat. Phenom.* **144–147C**, 1137–1143.

Lerotic, M., Jacobsen, C., Schäfer, T., and Vogt, S. (2004), Cluster analysis of soft x-ray spectromicroscopy data, *Ultramicroscopy* **100**, 35–57.

Leung, B. O., Hitchcock, A. P., Brash, J. L., Scholl, A., Doran, A., Henklein, P., Overhage, J., Hilpert, K., Hale, J. D., and Hancock, R. E. W. (2008), An X-ray spectromicroscopy study of competitive adsorption of protein and peptide onto polystyrene-poly (methyl methacrylate), *Biointerphases* **3**, F27–F35.

LeVan, P. D. and Beecken B. P. (2009), Hyperspectral opportunities with next-generation QSIP arrays, *Infrared Phys. Technol.* **52**, 361–363.

Lombi, E. and Susini, J. (2009), Synchrotron-based techniques for plant and soil science: Opportunities, challenges and future perspectives, *Plant Soil* **320**, 1–35.

Loo, Jr. B. W., Sauerwald, I. M., Hitchcock, A. P., and Rothman, S. S. (2001), A new sample preparation method for soft X-ray microscopy: Nitrogen based contrast and radiation tolerance properties of glycol methacrylate-embedded and sectioned tissue, *J. Microsc.* **204**, 69–86.

Marinkovic, N. S., Huang, R., Bromberg, P., Sullivan, M., Toomey, J., Miller, L. M., Sperber, E., Moshe, S., Jones, K. W., Chouparova, E., Lappi, S., Franzen, S., and Chance, M. R. (2002), Center for synchrotron biosciences' U2B beamline: An international resource for biological infrared spectroscopy, *J. Synchrotron Radiat.* **9**, 189–197.

Marinkovic, N. S., Adzic, A. R., Sullivan, M., Kovacs, K., Miller, L. M., Rousseau, D. L., Yeh, S. R., and Chance, M. R. (2000), Design and implementation of a rapid-mix flow cell for time-resolved infrared microspectroscopy, *Rev. Sci. Instrum.* **71**, 4057–4060.

Martin, M. C., Tsvetkova, N. M., Vrowe, J. H., and McKinney, W. R. (2001), Negligible sample heating from synchrotron infrared beam, *Appl. Spectrosc.* **55**, 111–113.

May, T., Ellis, T., and Reininger, R. (2007), Mid-infrared spectromicroscopy beamline at the Canadian Light Source. *Nucl. Instrum. Meth. Phys. Res. A* **582**, 111–113.

McClelland, J. F., Jones, R. W., and Bajic, S. J. (2002), FT-IR photoacoustic spectroscopy, in *Handbook of Vibrational Spectroscopy.*, Chalmers, J. and Griffiths, P. eds., Wiley, Hoboken, NJ.

Michaelian, K. H. (2003), *Photoacoustic Infrared Spectroscopy*, Wiley-Interscience, Hoboken, NJ.

Michaelian, K. H., May, T. E., and Hyett, C. (2008), Photoacoustic infrared spectroscopy at the Canadian Light Source: Commissioning experiments, *Rev. Sci. Instrum.* **79**, 1–5.

Miller, L. M. (2010), available at http://www.nsls.bnl.gov/newsroom/publications/otherpubs/imaging/workshopmiller.pdf.

Miller, L. M. and Dumas, P. (2006), Chemical imaging of biological tissue with synchrotron infrared light, *Biochim. Biophys. Acta* **1758**, 846–857.

Miller, L. M., Smith, G. D., and Carr, G. L. (2003), Synchrotron-based biological microspectroscopy: From the mid- to the far-infrared regimes, *J. Biol. Phys.* **29**, 219–230.

Miller, L. M. and Tague, T. J. (2002), Development and Biomedical Applications of Fluorescence assisted Synchrotron Infrared Micro-spectroscopy, *Vibrational Spectroscopy* **849**, 1–7.

Miller, L. M. and Smith, R. J. (2005), Synchrotrons vs. Globars, Point-Detectors vs. Focal Plane Arrays: Selecting the Best Source and Detector for Specific Infrared Microspectroscopy and Imaging Applications, Vibrational Spectroscopy, **38**, 237–240.

Mills, E. N. C., Parker, M. L., Wellner, N., Toole, G., Feeney, K., and Shewry, P. R. (2005), Chemical imaging: The distribution of ions and molecules in developing and mature wheat grain, *J. Cereal Sci.* **41**, 193–201.

Mitrea, G., Thieme, J., Guttmann, P., Heim, S., and Gleber, S. (2008), X-ray spectromicroscopy with the scanning transmission X-ray microscope at BESSY II, *J. Synchrotron Radiat.* **15**, 26–35.

Nasse, M. J., Reininger, R., Kubala, T., Janowski, S., and Hirschmugl, C. (2007), Synchrotron infrared microspectroscopy imaging using a multi-element detector (IRMSI-MED) for diffraction-limited chemical imaging, *Nucl. Instrum. Meth. Phys. Res., Sect. A* **58**, 107–110.

Naumann, D. (2002), Infrared spectroscopy in microbiology, in: Mayers, R. A. ed., *Encyclopedia of Analytical Chemistry*, Wiley, Chickesster, UK, pp. 102–131.

Naumann, D., Schultz, C.P., and Helm, D. (1996), What can infrared spectroscopy tell us about the structure and composition of intact bacterial cells? *In Infrared spectroscopy of biomolecules*, H.H. Mantsch and D. Chapman, eds., pp. 279–310. Wiley-Liss, New York.

Neu, T. R., Manz, B., Volke, F., Dynes, J. J., Hitchcock, A. P., and Lawrence, J. R. (2010), Advanced imaging techniques for assessment of structure, composition and function in biofilm systems, *FEMS Microbiol. Ecol.* **72**, 1–21.

Noll, F., Sumper, M., and Hampp, N. (2002), Nanostructure of diatom silica surfaces and of biomimetic analogues, *Nano Let.* **2**, 91–5.

Obst, M., Gasser, P., Mavrocordatos, D., and Dittrich, M. (2005), TEM-specimen preparation of cell/mineral interfaces by focused ion beam milling, *Am. Miner.* **90**, 1270–1277.

Obst, M., Dynes, J. J., Lawrence, J. R., Swerhone, G. D. W., Karunakaran, C., Kaznatcheev K. V., Bertwistle, D., Benzerara, K., Tyliszczak, T., and Hitchcock, A. P. (2009a), Precipitation of amorphous $CaCO_3$ (aragonite) controlled by cyanobacteria: A multi-technique study of the influence of EPS on the nucleation process, *Geochim. Cosmochim. Acta* **73**, 4180–4198.

Obst, M., Wang, J., and Hitchcock, A. P. (2009b), Soft X-ray spectro-tomography study of cyanobacterial biomineral nucleation, *Geobiology* **7**, 577–591.

Parkinson, D. Y., McDermott, G., Etkin, L. D, Le Gros, M. A., and Larabell, C. A. (2008), Quantitative 3-D imaging of eukaryotic cells using soft X-ray tomography, *J. Struct. Biol.* **162**, 380–386.

Pecher, K., Mccubbery, D., Kneedler, E., Rothe, J., Bargar, J., Meigs, G., Cox, L., Nealson, K., and Tonner, B. (2003), Quantitative charge state analysis of manganese biominerals in aqueous suspension using Scanning Transmission X-ray Microscopy (STXM). Geochim, *Cosmochim. Acta*, **67**, 1089–1098.

Rash, T. K. and Vogel, J. P. (2004), Ecological and agricultural applications of synchrotron IR microscopy, *Infrared Phys. Technol.* **45**, 393–341.

Rightor, E. G., Hitchcock, A. P., Ade, H., Leapman, R. D., Urquhart, S. G., Smith, A. P., Mitchell, G., Fischer, D., Shin, H. J., and Warwick, T. (1997), Spectromicroscopy of poly (ethylene terephthalate): Comparison of spectra and radiation damage rates in X-ray absorption and electron energy loss, *J. Phys. Chem. B* **101**, 1950–1961.

Rightor, E. G., Urquhart, S. G., Hitchcock, A. P., Ade, H., Smith, A. P., Mitchell, G. E., Priester, R. D., Aneja, R. D., Appel, G., Wilkes, G., and Lidy, W. E. (2002), Identification and quantitation of urea precipitates in flexible polyurethanes by X-ray spectromicroscopy, *Macromolecules* **35**, 5873–5882.

Russell, L. M., Maria, S. F., and Myneni, S. C. B. (2002), Mapping organic coatings on atmospheric particles, *Geophys. Res. Lett.* **29**, 26/21–26/ 24.

Schafer, T., Chanudet, V., Claret, F., and Filella, M. (2007), Spectromicroscopy mapping of colloidal/particulate organic matter in Lake Brienz, Switzerland, *Environ. Sci. Technol.* **41**, 7864–7869.

Schafer, T. Michel, P., Claret, F., Beetz, T., Wirick, S., and Jacobsen, C. (2009), Radiation sensitivity of natural organic matter: Clay mineral association effects in the Callovo-Oxfordian argillite, *J. Electron Spectrosc. Relat. Phenom.* **170**, 49–56.

Schumacher, M., Christl, I., Scheinost, A. C., Jacobsen, C., and Kretzschmar, R. (2005), Chemical heterogeneity of organic soil colloids investigated by scanning transmission X-ray microscopy and C-1s NEXAFS microspectroscopy, *Environ. Sci. Technol.* **39**, 9094–9100.

Smith, A. L. (1979), *Applied Infrared Spectroscopy: Fundamentals, Techniques and Analytical Problem-Solving*, Wiley, New York.

Stem, M. (2008), Understanding why researchers should use synchrotron-enhanced FTIR instead of traditional FTIR, *J. Chem. Educ.* **85**, 983–989.

Stewart-Ornstein, J., Hernández Cruz, D., Hitchcock, A. P., Hale, J, Overhage, J., Hilpert, K., Hancock, R, Dynes, J. J., Lawrence, J. R., Korber, D. R., and Leppard, G. G. (2006), *Predicting and Verifying NEXAFS Spectral Standards for STXM Mapping of Antimicrobial Peptides,* abstract, presented at Advanced Light Source Users Meeting, Berkeley, CA, Oct. 9–11, 2006.

Stöhr, J. (1992), *NEXAFS Spectroscopy*, Springer-Verlag, Berlin.

Szeghalmi, A., Kaminskyj, S., and Gough, K. M. (2007), A synchrotron FTIR microspectroscopy investigation of fungal hyphae grown under optimal and stressed conditions, *Anal. Bioanal. Chem.* **387**, 1729–1789.

Thieme, J, Gleber, S. C., Guttmann, P., Prietzel, J., McNulty, I., and Coates, J. (2008), Microscopy and spectroscopy with X-rays for studies in the environmental sciences, *Miner. Mag.* **72**, 211–216.

Thieme, J., McNult, I., Vogt, S., and Paterson, D. (2007), X-ray spectromicroscopy—a tool for environmental sciences, *Environ. Sci. Technol.* **41**, 6885–6889.

Thieme, J., Schneider, G., and Knochel, C. (2003), X-ray tomography of a microhabitat of bacteria and other soil colloids with sub-100 nm resolution, *Micron* **34**, 339–344.

Thomasson, J., Coin, C., Kahraman, H., and Fredericks, P. M. (2000), Attenuated total reflectance infrared microspectroscopy of coal, *Fuel* **79**, 591–718.

Toner, B., Fakra, S., Villalobos, N., Warwick, T., and Sposito, G. (2005), Spatially resolved characterization of biogenic manganese oxide production within a bacterial biofilm, *Appl. Environ. Mlicrobiol.* **71.** 1300–1310.

Vila-Comamala, J., Jefimovs, K., Pilvi, T., Ritala, M., Sarkar, S. S., Solak, H. H., Guzenko, V. A., Stampanoni, M., Marone, F, Raabe, J., Tzvetkov, G., Fink, R. H., Grolimund, D., Borca, C. N., Kaulich, B., and David, C. (2009), Advanced X-ray diffractive optics, *J. Phys. Conf. Ser.* **186**, 1–3.

Wang, J., Botton, G. A., West, M. M., and Hitchcock, A. P. (2009a), Quantitative evaluation of radiation damage to polyethylene terephthalate by soft X-rays and high energy electrons, *J. Phys. Chem. B* **113**, 1869–1876.

Wang, J., Morin, C., Li, L., Hitchcock, A. P., Zhang, X., Araki, T., Doran, A., and Scholl, A. (2009b), Radiation damage in soft X-ray microscopy, *J. Electron Spectrosc. Relat. Phenom.* **170**, 25–36.

Yoon, T. H., Benzerara, K., Ahn, S., Luthy, R. G., Tyliszczak, T., and Brown G. E. (2006), Nanometer-scale chemical heterogeneities of black carbon materials and their impacts on PCB sorption properties: Soft X-ray spectromicroscopy study, *Environ. Sci. Technol.* **40**, 5923–5929.

Yu, P. (2007), Microlocalization and distribution of digestion-resistant aromatic lignin and cellulosic compounds in feeds at cellular and subcellular levels: A novel approach, *J. Animal Feed Sci.* **16**, 505–525.